CLASSIFICATION
Major: BIOLOGICAL SCIENCES. Anthropology.
Minor. PHYSICAL SCIENCES. Geology.

Aridity and hominin environments

Scott A. Blumenthal[a]*, Naomi E. Levin[b], Francis H. Brown[c], Jean-Philip Brugal[d], Kendra L. Christz[e], John M. Harris[f], Glynis E. Jehle[c], Thure E. Cerling[c,e]

Affiliations:

[a] Research Laboratory for Archaeology, University of Oxford, Oxford UK.
[b] Department of Earth & Environmental Sciences, University of Michigan, Ann Arbor, MI USA.
[c] Department of Geology & Geophysics, University of Utah, Salt Lake City, UT USA.
[d] Laboratoire Méditerranéen de Préhistoire Europe Afrique, UMR 7269, CNRS, Aix-Marseille Université, 13094 Aix-en-Provence Cedex 2, France.
[e] National Museum of Natural History, Smithsonian Institution, Washington DC USA.
[f] Natural History Museum of Los Angeles County, Los Angeles, CA USA.

*Correspondence to: scott.blumenthal@arch.ox.ac.uk

ABSTRACT

Aridification is often considered a major driver of long-term ecological change and hominin evolution in eastern Africa during the Plio-Pleistocene. However, this hypothesis remains inadequately tested due to difficulties in reconstructing terrestrial paleoclimate. We present a revised aridity index for quantifying water deficit in terrestrial environments using tooth enamel $\delta^{18}O$ values, and we use this approach to address paleoaridity over the past 4.4 million years in eastern Africa. We find no long-term trend in water deficit, consistent with other terrestrial climate indicators in the Omo-Turkana Basin, and no relationship between paleoaridity and herbivore paleodiet structure among fossil collections meeting the criteria for water deficit estimation. Thus, we suggest that changes in the abundance of C_4 grass and grazing herbivores in eastern Africa during the Pliocene and Pleistocene may have been decoupled from aridity. As in modern African ecosystems, other factors such as rainfall seasonality or ecological interactions among plants and mammals may be important for understanding the evolution of C_4 grass- and grazer-dominated biomes.

SIGNIFICANCE STATEMENT.

Oxygen isotopes in modern and fossil mammals can provide information on climate. In this study, we provide a new record of aridity experienced by early hominins in Africa. We show that past climates were similar to the climate in eastern Africa today, and that early hominins experienced highly variable climates over time. Unexpectedly, our findings suggest that the long-term expansion of grasses and grazing herbivores since the Pliocene, a major ecological transformation thought to drive aspects of hominin evolution, was not coincident with aridification in northern Kenya. This finding raises the possibility that some aspects of hominin environmental variability may have been uncoupled from aridity, and may instead be related to other factors such as rainfall seasonality or ecological interactions among plants and mammals.

\body
A central challenge of human evolutionary studies is understanding the role of climatic change in shaping early hominin environments and selective pressures (1, 2). Aridity influences the distribution and abundance of vegetation in African environments (3), and changes in aridity over both long and short time scales have been suggested to drive changes in hominin environments leading to adaptation, dispersal, speciation, and extinction (2, 4, 5). The notion that aridity may have driven certain adaptations has been fundamental to discussions of hominin evolution since 1925 (6), and continues to feature prominently in studies addressing changes in hominin locomotion, body proportions, thermoregulation, food acquisition, tool use, and social organization (7-10).

Changes in African climate are driven principally by changes in Earth's orbital geometry, which has been documented in the geologic past using marine and continental sedimentary records (4, 11-15). Marine core records of dust, leaf wax biomarkers, pollen, and sapropels indicate long-term aridification across Africa since the late Miocene (4, 12, 14, 16-18), which has been linked to global cooling (19), changes in ocean circulation and temperature gradients (20), high latitude glaciation (4), low latitude atmospheric circulation (14), and tectonic uplift (21). Increasing aridity has been thought to drive the origin and subsequent expansion of C_4 plants (grasses and sedges) (22). The long-term increase in abundance of C_4 plants throughout the Pliocene and Pleistocene is well documented in eastern Africa using carbon isotope ratios in pedogenic carbonates and leaf wax biomarkers (23, 24) and coincides with increasing reliance on C_4-based resources among mammals, including hominins and other primates (25, 26). Variation in the timing of vegetation change across basins indicates that existing continental- and regional-scale climate records are not sufficient to understand the drivers of basin- and local-scale ecological change, and do not reflect local hominin environments (23, 27). Evidence for

vegetation changes with precession-scale timing suggests direct climate forcing of such changes over thousands of years (28, 29), but drivers of environmental change may not be equivalent at short versus long time scales and may also vary through time.

Uncertainties in the relationships between climate and hominin environments stem in part from problems in reconstructing terrestrial aridity. Terrestrial climate indicators commonly used in eastern Africa, including the isotopic composition of pedogenic carbonates (21, 27, 30), mammal taxonomy (31-33) and morphology (34), provide valuable insights into past environments but are sensitive to multiple environmental and evolutionary changes such that it can be difficult to identify the specific role of aridity. Additionally, existing faunal records (31-34) typically combine fossils from multiple sites and may integrate relatively long (but varying) periods of time. Other climate proxies, such as the deuterium isotope composition of leaf wax biomarkers (17) and fossil leaf morphology (35) have not been widely applied in Pliocene-Pleistocene sequences in Africa.

In the present study, we address paleoaridity using oxygen isotope ratios ($\delta^{18}O$) in herbivore tooth enamel. Our goal is to investigate the role of climate in shaping hominin environments over the past 4.4 million years, concentrating on individual stratigraphic horizons associated with hominin fossil and archaeological material. We focus on the Omo-Turkana Basin, where sediments preserve abundant evidence of early hominin evolution and associated environments throughout the Pliocene and Pleistocene. The environmental history of this basin is not necessarily representative of eastern Africa (1), but nonetheless provides a useful study system for investigating interactions between climate and ecology. A major benefit of analyzing herbivore tooth enamel is the possibility of comparing paired oxygen and carbon isotope records from the same fossil collections where hominin specimens or stone tools have been found,

providing indicators of climate and ecology at spatial scales directly relevant to hominin environments. However, we cannot address short-term orbital scale environmental variability, due to discontinuous sedimentation associated with terrestrial vertebrate fossil collections.

Our geochemical approach for quantifying aridity in tropical African ecosystems relies on differing oxygen isotopic effects among taxa that are evaporation-sensitive (ES) and evaporation-insensitive (EI) (36, 37). This method, which builds on earlier work that focused on oxygen isotope variation among individual taxa (38-42), relies on a comparison of multiple taxa and simultaneously accounts for isotopic variation related to changes in both climate and environmental water. This proxy has advantages over previously used paleoaridity indicators because it is largely insensitive to changes in: (*i*) vegetation, which control mammal taxonomic abundances, diet, and carbon isotopic records from tooth enamel, soil carbonates, and leaf wax biomarkers; (*ii*) moisture source, soil temperature, and elevation, which influence oxygen isotopic records reflecting meteoric water such as soil carbonates and leaf wax biomarkers; and (*iii*) mammal physiology and behavior, which affect oxygen isotopic records of individual species. Previous applications of this approach to the African fossil record have been hampered by uncertainties in the selection of appropriate taxa and the unavailability of appropriate fossil collections.

Aridity is expressed as water deficit, which describes the annual difference (mm/y) between water loss (evaporation and transpiration) and gain (precipitation) and is a useful indicator of water availability in African ecosystems (43, 44). $\delta^{18}O$ values in large mammalian herbivore tooth enamel are in equilibrium with body water, which reflects oxygen inputs from food, drinking water, and air, and ultimately relate to meteoric (precipitation-derived) water (45). In the tropics, the oxygen isotopic composition of meteoric water relates to rainfall amount,

elevation, and moisture source (46). Evaporation enriches remaining water in the heavy isotope ^{18}O relative to source water, such that aridity can be quantified by comparing one isotopic record that tracks meteoric water with another that tracks evaporative enrichment (36, 37).

The aridity index (36) is based on regressions between water deficit and the oxygen isotopic enrichment between tooth enamel and local meteoric water ($\varepsilon_{enamel\text{-}mw}$). Mammalian herbivore taxa for which $\varepsilon_{enamel\text{-}mw}$ increases with water deficit are classified as ES, and taxa for which $\varepsilon_{enamel\text{-}mw}$ does not change with water deficit are classified as EI. Meteoric water cannot be measured directly in the fossil record; therefore, these relationships can be extended to the fossil record to predict water deficit by using $\delta^{18}O$ values of EI taxa to represent meteoric water because $\varepsilon_{ES\text{-}EI}$ and $\varepsilon_{ES\text{-}mw}$ track aridity (36). Applying the aridity index to the fossil record requires the assessment of appropriate taxa, geological context, diagenetic alteration, and sample size (SI Appendix).

To revise the aridity index, we present a compilation of new and previously published $\delta^{18}O$ values (n = 1224 in 57 species) measured on tooth enamel from modern mammalian herbivores from 37 locations in eastern and central Africa (Fig. 1), climate data and water deficit estimates for each location, and $\delta^{18}O$ values in meteoric water (n = 161) from 33 of these locations (Table S1, Datasets S1-2). Our compilation significantly expands on a previously published dataset (36) and includes $\delta^{18}O$ data from many more locations and taxa, and it also expands the water deficit scale due to the correction of a mathematical error in calculating potential evapotranspiration (Fig. S1; SI Appendix). To address paleoaridity in eastern Africa, we present a compilation of new and previously published mammalian herbivore $\delta^{18}O_{enamel}$ values (n = 273) from 26 fossil collections (Fig. 1) 4.4 to 0.01 million years in age, which were chosen based on the potential for addressing paleoaridity and association with hominin fossil and

archaeological material (Dataset S3). We use a subset of $\delta^{18}O_{enamel}$ values (n = 160) from 11 fossil collections in the Omo-Turkana Basin, including specimens from the Kanapoi, Koobi Fora, Nachukui, and Kibish Formations (Fig. 1, Fig. S3), that meet criteria for the application of the aridity index to evaluate long-term changes in paleoaridity in this basin. We also estimate paleoaridity using previously published $\delta^{18}O_{enamel}$ values from two eastern African fossil collections outside the Turkana Basin that meet criteria for applying this method, including Aramis, Ethiopia (4.4 Ma) and Kanjera South, Kenya (2.0 Ma). Finally, we investigate the relationship between aridity and ecosystem structure in eastern Africa using a compilation of previously published modern mammalian herbivore tissue $\delta^{13}C$ values (n > 1600) (25) and a compilation of new and previously published fossil tooth enamel $\delta^{13}C$ values (n = 658) from fossil collections with paleoaridity estimates.

RESULTS AND DISCUSSION

Terrestrial aridity proxy. Across modern localities, water deficit increases non-linearly with decreasing mean annual precipitation (logarithmic regression, $r^2 = 0.7546$, $p < 0.0001$) and increasing mean annual temperature (quadratic polynomial regression, $r^2 = 0.6829$, $p < 0.0001$) (Fig. S1). $\varepsilon_{enamel\text{-}mw}$ values for Hippopotamidae, Elephantidae, and Rhinocerotidae do not vary with water deficit and these taxa are classified as evaporation insensitive (Fig. 2A). $\varepsilon_{enamel\text{-}mw}$ values for Giraffidae, Hippotragini, and Tragelaphini increase with water deficit and these taxa are classified as evaporation sensitive (Fig. 2B). The slopes of WD-$\varepsilon_{ES\text{-}mw}$ regressions vary significantly from each other ($p < 0.05$, F-test), except for Giraffidae and Hippotragini ($p > 0.05$, F-test). Despite preliminary observations to the contrary (36), the addition of more locations in this dataset reveals that Antilopini, Bovini, and Neotragini should be excluded from the ES

category (Fig. 2C). Other sampled bovids, suids, and equids (Fig. 2C) have no significant relationship with water deficit ($p > 0.05$), except Cephalophini ($p < 0.05$), which are not considered further due to $\varepsilon_{enamel\text{-}mw}$ values that are more variable and/or span a restricted water deficit range. Additional data are needed to address variability in $\varepsilon_{enamel\text{-}mw}$ values across bovid genera, although many bovid fossils are identifiable only to tribe.

We use a body water model to identify possible physiological and behavioral mechanisms driving the relationship between $\varepsilon_{enamel\text{-}mw}$ and water deficit among EI and ES taxa (see Supplementary Materials). A static oxygen budget, where body water is only influenced by changes in the isotopic composition of oxygen influxes rather than changes in the balance of influxes, is inconsistent with $\varepsilon_{enamel\text{-}mw}$ of either ES or EI taxa (Fig. S2C and D). Therefore, ^{18}O enrichment of leaf water in arid environments is insufficient to explain the relationship between $\varepsilon_{enamel\text{-}mw}$ values and water deficit among ES taxa. Instead, sensitivity to evaporation likely relates to differences in drinking behavior and associated changes in the balance of oxygen influxes as the environment varies. Predicted $\varepsilon_{enamel\text{-}mw}$ values suggest that EI taxa reflect meteoric water as aridity increases due to a balance between increasing drinking water and decreasing food water (Fig. S2C), and ES taxa track increasing aridity due to a balance between decreasing drinking water and increasing intake of food water and O_2 (both of which are sensitive to evaporation) (Fig. S2D).

The aridity index is the relationship between water deficit and the enrichment between ES and EI taxa ($\varepsilon_{ES\text{-}EI}$). Significant WD-$\varepsilon_{ES\text{-}EI}$ regressions ($p < 0.05$) that can be used to estimate paleoaridity include $\varepsilon_{Giraffid\text{-}Hippopotamidae}$, $\varepsilon_{Tragelaphini\text{-}Hippopotamidae}$, $\varepsilon_{Hippotragini\text{-}Hippopotamidae}$, $\varepsilon_{Tragelaphini\text{-}Elephantidae}$, and $\varepsilon_{Tragelaphini\text{-}Rhinocerotidae}$ (Fig. 3 and Table S4). The standard errors of these regression models are relatively low (±193 mm/y to ±478.1 mm/y) and coefficients of determination are

high (r^2 = 0.81 to 0.92), and as a result these models have sufficient predictive power to estimate paleoaridity in the fossil record. Slopes are different among WD-$\varepsilon_{ES\text{-}EI}$ regressions ($p < 0.05$, F test); therefore, a pooled or common slope as previously suggested (36) is not appropriate. We use the mean of water deficit values calculated with WD-$\varepsilon_{ES\text{-}EI}$ regressions for all available ES-EI pairs from each fossil collection. Uncertainty in WD estimates (~800 mm/y) corresponds to ~20% of the WD range in modern eastern African environments, sufficient to detect long-term trends in Turkana (SI Appendix). Other WD-$\varepsilon_{ES\text{-}EI}$ regressions are not significant ($p > 0.05$) and should not be used to estimate paleoaridity.

Paleoaridity. Oxygen isotope analyses of fossil tooth enamel for paleoaridity estimation were restricted to fossil collections with well-defined stratigraphic and sedimentological context and the preservation of appropriate ES and EI taxa. Among all fossil collections used to evaluate paleoaridity, we find highly variable conditions including both mesic (WD < 0) and arid (WD > 0) climates that fall within a WD range (~ -550-1700 mm/y) encompassing ~61% of the modern range (Fig. 4 and Fig. S4). The mean water deficit estimated by fossil tooth enamel is 471 mm/y, which is similar to ($p > 0.05$) present-day mean water deficit in eastern and central Africa (251 mm/y) (Figs. S1 and S4, Tables S1 and S3). Among fossil collections from the Omo-Turkana Basin, we detect no long-term trend in water deficit between ~4.2 and 0.01 million years ago ($p > 0.05$) (Fig. 4).

The paleoaridity record (Fig. 4 and Fig. S4) begins in the Pliocene with a highly uncertain estimate of arid conditions associated with *Ardipithecus ramidus* fossils from the Lower Aramis Member, Sangatole Formation (~4.4 Ma) (47). In the Omo-Turkana Basin, we find arid conditions at Kanapoi (~4.16 Ma) and a highly uncertain estimate of mesic conditions

at Allia Bay (~4.0 Ma), both associated with *Australopithecus anamensis* (48) and pedogenic carbonate $\delta^{13}C$ values indicative of vegetation ranging from woodland/bushland/shrubland to wooded grassland (49). Mid- to late-Pliocene (~3.5-2.8 Ma) fossil collections in Turkana indicate variable conditions that include arid (Kangatukuseo KU1) and arid to mesic (Lomekwi LO4/5) climates, associated with pedogenic carbonate $\delta^{13}C$ values indicating woody cover including woodland/bushland/shrubland (Fig. 4) (49). This time interval in Turkana includes fossils of the hominin genera *Kenyanthropus* and *Paranthropus* (Table S2). The early Pleistocene (~2.5-1.5 Ma) is represented in the Turkana Basin by fossil assemblages in the upper Burgi Member of the Koobi Fora Formation as well as the Kaito Member of the Nachukui Formation, which indicate arid (FwJj20 and Kalochoro KL3/6, Naiyena Engol NY2/3), nearly balanced (Kokiselei KS2 and Kangatukuseo KU2/3), and mesic (Kokiselei KS1) conditions. Pedogenic carbonate $\delta^{13}C$ values indicate that relatively open vegetation, including wooded grasslands, became more prevalent during this time interval in Turkana (49), which includes an abundant fossil record of *Homo* and *Paranthropus* (Table S2). Mesic conditions prevailed at Kanjera South KS-2 in southwestern Kenya, associated with an open grassland ecosystem (50). Archaeological occurrences at Kanjera South, as well as in the Nachukui and Koobi Fora Formations in the Turkana Basin, demonstrate that Oldowan toolmaking hominins inhabited mesic and arid environments (Fig. S4). The late Middle Pleistocene to Holocene (~0.2-0.01 Ma) is represented in the Turkana Basin by fossil assemblages in the Kibish Formation, which indicate arid conditions in Member 4 and arid to mesic conditions in Member 1. Fossils identified as *Homo sapiens* (Omo I and Omo II) are from Member 1, and other human specimens are derived either from Member 3 or 4 (Table S2). Water deficit estimates in Members 1 and 4

are substantially lower than Turkana today, consistent with deposition during relatively humid periods associated with high lake levels and sapropel formation intervals (51).

Relationships between climate and ecology. To understand the significance of aridity for shaping hominin environments in eastern Africa, we further consider the relationship between climate and ecology in modern African ecosystems. Vegetation in Africa is shaped by complex interactions between multiple abiotic (rainfall amount and seasonality, fire, atmospheric pCO_2) and biotic (herbivory) factors, and the relative importance of these factors is contingent on the ecological history of each area (52-54). Although woody cover is constrained by aridity (55), vegetation does not respond in a direct or continuous manner to changes in annual rainfall, and each biome (forest, savanna, grassland) is distributed over a wide rainfall range (1000-3000 mm/y) (52, 56, 57). We find that among modern eastern and central African ecosystems, the proportion of C_4 grazers increases with water deficit ($p = 0.00536$, $r^2 = 0.262$) and the proportion of C_3 browsers decreases with water deficit ($p = 0.021$, $r^2 = 0.1884$) (Fig. 5). However, these correlations are weak, and during the Pliocene-Pleistocene forests were rare in the Turkana Basin (25, 27, 49, 58) and elsewhere in eastern Africa (23). After excluding forests, we find no relationship between water deficit and the proportional abundance of each diet guild (Fig. 5). Thus, although the abundance of C_4 plants and C_4 grazing herbivores are often used as an indicators of aridity (21, 30), variation in C_4 biomass among non-forest biomes can be decoupled from aridity.

Paleoaridity records from $\delta^{18}O$ of tooth enamel provide a means to investigate links between climate and ecology in hominin environments, but are also highly discontinuous due to the incompleteness of the terrestrial fossil record, compounded in this case by the scarcity of

fossil assemblages meeting the criteria for applying the aridity index. We address this problem in three ways. First, we examine the fidelity of long-term environmental records derived from the fossil collections used for paleoaridity analysis. The long-term increase in the proportion of C_4 grazers among Artiodactyla-Perissodactyla-Proboscidea over the Pliocene-Pleistocene in the Omo-Turkana Basin is similar ($p > 0.05$, *F* test) when calculated using tooth enamel $\delta^{13}C$ values from paleoaridity fossil collections ($p = 0.02324$, $r^2 = 0.3868$) or from a larger fossil tooth enamel $\delta^{13}C$ dataset divided into long time bins (>100 ka) ($p = 0.0006911$, $r^2 = 0.7391$) (Fig. S5). Therefore, it is possible to recover first-order environmental trends using fossils from these discontinuous depositional intervals.

Second, we compare our water deficit record with previously published geological and faunal-based reconstructions of terrestrial paleoclimate in Turkana with varying time representation and analytical biases. There are no trends in paleoclimate based on paleosol calcic depth, mammal hypsodonty and lophedness (k-nearest neighbor model), or bovid tribe abundance (Fig. S6). Estimated precipitation decreases over time based on mammal community structure ($p = 0.03258$, $r^2 = 0.2295$) and mammal hypsodonty and lophedness (linear regression model) ($p = 0.004477$, $r^2 = 0.0583$), but these trends are weak and based on proxies influenced by evolutionary and dietary change, respectively, that may not be related to aridity (Fig. S6). Taken together, evidence for marked long-term aridification in the Turkana Basin is weak.

Third, we examine the relationship between water deficit and ecology in the fossil record, irrespective of time. There are no relationships ($p > 0.05$) between water deficit and the proportion of C_4 grazers, C_3-C_4 mixed feeders, or C_3 browsers (Fig. 5 and Table S4). Due to the lack of suitable fossil collections for the application of our tooth enamel aridity proxy, we do not address climate prior to ~4 Ma. The Late Miocene appears to have been more humid in Turkana

and elsewhere (34), although aridification prior to ~4 Ma predates the long-term increase in C_4 vegetation and C_4 grazing mammalian herbivore that continues throughout the Pliocene and Pleistocene (25, 27).

Despite coarse time resolution associated with the tooth enamel $\delta^{18}O$ water deficit calculations, we suggest that the Pliocene-Pleistocene expansion in C_4 plants and C_4 grazing herbivores appears not to be coincident with significant long-term aridification in the Omo-Turkana Basin (Fig. 4, Fig. S6). The possibility of a smaller long-term increase in aridity, undetected due to uncertainty in water deficit estimates, cannot be discounted but would not necessarily have been a major environmental driver since ecological feedbacks in African biomes inhibit vegetation responses to climate change (52-54). Thus, the cause of the major long-term expansion of C_4 biomass within Turkana and elsewhere remains unclear, but may relate climatic and ecological dynamics unrelated to annual water deficit and that need not be equivalent across basins or regions (1, 23, 25). Our results do not preclude the possibility of climate-driven change in hominin environments generally, but highlight the need to address possible variability in the determinants of environmental change in different areas, as basins do not necessarily respond in a straightforward way to continental- and regional-scale aridification. Similarly, previous paleosol and leaf wax biomarker paleovegetation studies demonstrate that the timing and magnitude of the expansion of C_4 plants is not uniform across eastern and northeastern Africa (23, 27, 59). Thus, climatic and ecological dynamics appear to vary across basins, and regional-scale climate proxies must be contextualized by terrestrial, basin-scale environmental records most relevant to hominin evolution.

Our aridity record is consistent with the notion that climate instability may be an important driver of hominin evolution (2, 30). Arid conditions were prevalent during two large

lake intervals ~4.0 and 2.0 Ma (Fig. 4), consistent with climate variability including periods of increased aridity occurring within generally humid periods characterized by widespread lake formation (30). Orbital-scale environmental change has been demonstrated using leaf wax biomarkers from Early Pleistocene lake sediments at Olduvai Gorge, suggesting a direct link between rainfall and changes in the balance of woody and grassy vegetation (28). This case, and other episodes of climate-driven vegetation change (29, 60), are entirely consistent with ecological dynamics in cases where woody cover is not constrained by other factors, or when drastic changes in precipitation, particularly during periods of heightened climatic variability, exceed thresholds for stable biome states otherwise maintained by herbivory, fire, or other factors (44, 53).

Aridity and human evolution. Our paleoaridity record demonstrates that hominins were able to accommodate variable environments throughout the Pliocene-Pleistocene in eastern Africa, and is consistent with the notion that biological and behavioral changes in hominins, including upright posture, hair loss, sweating, and long-distance scavenging or running, may relate to thermophysiological challenges associated with surviving periodically arid conditions and high heat loads (58). The relative abundance of C_3 woody vegetation during the Pliocene (Fig. 4) is consistent with the notion that early bipedal hominins could have relied on areas with shade-providing plants that may have reduced water- and heat-stress. Archaeological occurrences in Turkana during the early Pleistocene (~2.4-1.4 Ma) are preferentially associated with lower $\delta^{13}C$ values of paleosol carbonate compared to those from non-archaeological deposits, indicating that hominins concentrated their activities in more wooded areas (61). In contrast, archaeological occurrences at Kanjera South, southwestern Kenya (2.0 Ma) demonstrate hominins repeatedly

using an open grassland (50) when aridity was low (Fig. S4). Thus, early hominin land use patterns were likely structured by the interplay between aridity and vegetation, such that the exploitation of increasingly open C_4-dominated ecosystems may have been limited during periods of high aridity due to constraints on the availability of water and shade.

Conclusions

Our findings demonstrate how mammal tooth enamel $\delta^{18}O$ values can be used to quantify paleoaridity directly associated with the hominin fossil and archaeological record. Water deficit values estimated from fossil tooth enamel $\delta^{18}O$ values suggest that early hominins experienced highly variable climatic conditions within the range of present-day environments in the region, and could accommodate arid conditions as early as ~4.2 million years ago. The modern hyperarid climate in Turkana is not a useful analog for paleoaridity in the basin. The lack of evidence for marked, long-term aridification, and the absence of any relationship between aridity and herbivore diet structure, suggests that other abiotic or biotic determinants may have driven long-term ecological restructuring in the Omo-Turkana Basin. The complex interplay of ecology and behavior suggests that disentangling the influence of climate on the evolution of humans and other mammals remains a significant challenge. Future inter- and intra-basinal studies are needed to investigate relationships between changing basinal geometry, biogeography, climate, depositional setting, ecology, and evolution.

Methods and materials

Additional details on isotopic and statistical methods, water deficit calculations, models of leaf water, leaf cellulose, and body water $\delta^{18}O$, and an expanded discussion on criteria for the

application of the aridity index are provided in the SI. Modern meteoric water samples were compiled from the literature (see Dataset S1). Modern and fossil samples of mammalian tooth enamel were analyzed for $\delta^{18}O$ using standard methods, or were compiled from the literature (SI Appendix and Datasets S2 and S3). Information on the geological context of fossil specimens is available in the SI and Dataset S3.

ACKNOWLEDGEMENTS. This study was made possible by geological and paleontological fieldwork in the Omo-Turkana Basin over the last 50 years. Fossil collection was in collaboration with Anna K. Behrensmeyer, David R. Braun, Meave G. Leakey, as well as the West Turkana Archaeological Project. We thank the National Museums of Kenya, particularly Idle Farah, Emma Mbua, Fredrick Manthi, Purity Kiura, and Mary Muungu, for support and for facilitating access to fossil specimens. We also extend our gratitude to other researchers and staff for fossil preparation. Many organizations have offered assistance and access to collections, including the American Museum of Natural History, the Centre de Recherche en Science Naturelles of the Democratic Republic of Congo, Kenya Wildlife Service, Save the Elephants, the Turkana Basin Institute, and the Uganda Wildlife Authority. Thanks to Tom Plummer for reading a previous draft of this manuscript, and to Faysal Bibi and Scott Jasechko for sharing data. This research was funded by the Geological Society of America, Leakey Foundation, National Geographic Society (YEG 9349-13), National Science Foundation (0617010, 0621542, 1260535), Sigma Xi, and the Wenner-Gren Foundation (8694). Data used in this paper are available in the Supplementary Materials.

REFERENCES

1. Levin NE (2015) Environment and Climate of Early Human Evolution. *The Annual Review of Earth and Planetary Sciences* 43:405–429.

2. Potts R (2013) Hominin evolution in settings of strong environmental variability.

Quaternary Science Reviews 73:1–13.

3. Bond WJ (2008) What Limits Trees in C_4 Grasslands and Savannas? *The Annual Review of Ecology, Evolution, and Systematics* 39(1):641–659.

4. deMenocal PB (2004) African climate change and faunal evolution during the Pliocene-Pleistocene. *Earth and Planetary Science Letters* 220:3–24.

5. Shultz S, Maslin M (2013) Early human speciation, brain expansion and dispersal influenced by African climate pulses. *PLoS ONE* 8(10):e76750.

6. Dart RA (1925) *Australopithecus africanus*: The Man-Ape of South Africa. *Nature* 115:195–199.

7. Bramble D, Lieberman D (2004) Endurance running and the evolution of *Homo*. *Nature* 432:345–352.

8. Ruxton GD, Wilkinson DM (2011) Avoidance of overheating and selection for both hair loss and bipedality in hominins. *Proceedings of the National Academy of Sciences* 108(52):20965–20969.

9. O'Connell JF, Hawkes K, Blurton Jones NG (1999) Grandmothering and the evolution of *Homo erectus*. *Journal of Human Evolution* 36(5):461–485.

10. Ruff CB (1993) Climatic adaptation and hominid evolution: the thermoregulatory imperative. *Evolutionary Anthropology* 2:53–60.

11. Tiedemann R, Sarnthein M, Shackleton NJ (1994) Astronomic timescale for the Pliocene Atlantic $\delta^{18}O$ and dust flux records of Ocean Drilling Program Site 659. *Paleoceanography* 9(4):619–638.

12. Larrasoaña JC, Roberts AP, Rohling EJ, Winklhofer M, Wehausen R (2003) Three million years of monsoon variability over the northern Sahara. *Clim Dyn* 21(7-8):689–698.

13. Rossignol-Strick M (1983) African monsoons, an immediate climate response to orbital insolation. *Nature* 304(5921):46–49.

14. Trauth MH, Larrasoaña JC, Mudelsee M (2009) Trends, rhythms and events in Plio-Pleistocene African climate. *Quaternary Science Reviews* 28(5-6):399–411.

15. Kingston JD, Deino AL, Edgar R, Hill A (2007) Astronomically forced climate change in the Kenyan Rift Valley 2.7-2.55 Ma: implications for the evolution of early hominin ecosystems. *Journal of Human Evolution* 53(5):487–503.

16. Dupont LM, Rommerskirchen F, Mollenhauer G, Schefuß E (2013) Miocene to Pliocene changes in South African hydrology and vegetation in relation to the expansion of C_4 plants. *Earth and Planetary Science Letters* 375:408–417.

17. Liddy HM, Feakins SJ, Tierney JE (2016) Cooling and drying in northeast Africa across the Pliocene. *Earth and Planetary Science Letters* 449:430–438.

18. Bonnefille R (2010) Cenozoic vegetation, climate changes and hominid evolution in tropical Africa. *Global and Planetary Change* 72:390–411.

19. Zachos JC, Pagani M, Sloan L, Thompson E, Billups K (2001) Trends, Rhythms, and Aberrations in Global Climate 65 Ma to Present. *Science* 292:686–693.

20. Cane MA, Molnar P (2001) Closing of the Indonesian seaway as a precursor to east African aridification around 3–4 million years ago. *Nature* 411(6834):157–162.

21. Sepulchre P (2006) Tectonic Uplift and Eastern Africa Aridification. *Science* 313(5792):1419–1423.

22. Edwards EJ, et al. (2010) The origins of C_4 grasslands: integrating evolutionary and ecosystem science. *Science* 328(5978):587–591.

23. Uno KT, Polissar PJ, Jackson KE, deMenocal PB (2016) Neogene biomarker record of vegetation change in eastern Africa. *Proceedings of the National Academy of Sciences* 113(23):6355–6363.

24. Feakins SJ, Levin NE, Liddy HM, Sieracki A (2013) Northeast African vegetation change over 12 my. *Geology* 41:295–298.

25. Cerling TE, et al. (2015) Dietary changes of large herbivores in the Turkana Basin, Kenya from 4 to 1 Ma. *Proceedings of the National Academy of Sciences* 112(37):11467–11472.

26. Levin NE, Haile-Selassie Y, Frost SR, Saylor BZ (2015) Dietary change among hominins and cercopithecids in Ethiopia during the early Pliocene. *Proceedings of the National Academy of Sciences* 112:12304–12309.

27. Levin NE, Brown FH, Behrensmeyer AK, Bobe R, Cerling TE (2011) Paleosol carbonates from the Omo Group: Isotopic records of local and regional environmental change in East Africa. *Palaeogeography Palaeoclimatology Palaeoecology* 307:75–89.

28. Magill CR, Ashley GM, Freeman KH (2013) Ecosystem variability and early human habitats in eastern Africa. *Proceedings of the National Academy of Sciences* 110:1167–1174.

29. Rose C, Polissar PJ, Tierney JE, Filley T, deMenocal PB (2016) Changes in northeast African hydrology and vegetation associated with Pliocene–Pleistocene sapropel cycles. *Philosophical Transactions of the Royal Society B: Biological Sciences* 371(1698):20150243.

30. Maslin MA, et al. (2014) East African climate pulses and early human evolution. *Quaternary Science Reviews* 101:1–17.

31. Bibi F, Kiessling W (2015) Continuous evolutionary change in Plio-Pleistocene mammals of eastern Africa. *Proceedings of the National Academy of Sciences* 112:10623–10628.

32. Bobe R (2006) The evolution of arid ecosystems in eastern Africa. *Journal of Arid Environments* 66(3):564–584.

33. Fernández MH, Vrba ES (2006) Plio-Pleistocene climatic change in the Turkana Basin (East Africa): Evidence from large mammal faunas. *Journal of Human Evolution* 50(6):595–626.

34. Fortelius M, et al. (2016) An ecometric analysis of the fossil mammal record of the Turkana Basin. *Philosophical Transactions of the Royal Society B: Biological Sciences* 371(1698):20150232.

35. Peppe DJ, et al. (2011) Sensitivity of leaf size and shape to climate: global patterns and paleoclimatic applications. *New Phytologist* 190(3):724–739.

36. Levin NE, Cerling TE, Passey BH, Harris JM, Ehleringer JR (2006) A stable isotope aridity index for terrestrial environments. *Proceedings of the National Academy of Sciences* 103(30):11201–11205.

37. Kohn MJ, Schoeninger MJ, Valley JW (1996) Herbivore tooth oxygen isotope compositions: Effects of diet and physiology. *Geochimica et Cosmochimica Acta* 60:3889–3896.

38. Ayliffe LK, Chivas AR (1990) Oxygen isotope composition of the bone phosphate of Australian kangaroos: Potential as a palaeoenviromental recorder. *Geochimica et Cosmochimica Acta* 54:2603–2609.

39. Ayliffe LK, Lister A, Chivas AR (1992) The preservation of glacial-interglacial climatic signatures in the oxygen isotopes of elephant skeletal phosphate. *Palaeogeography Palaeoclimatology Palaeoecology* 99:179–191.

40. Luz B, Cormie AB, Schwarcz HP (1990) Oxygen isotope variations in phosphate of deer bones. *Geochimica et Cosmochimica Acta* 54:1723–1728.

41. Huertas AD, Iacumin P, Stenni B, Chillión B, Longinelli A (1995) Oxygen isotope variations of phosphate in mammalian bone and tooth enamel. *Geochimica et Cosmochimica Acta* 59:4299–4305.

42. Cormie A, Luz B, Schwarcz H (1994) Relationship between the hydrogen and oxygen isotopes of deer bone and their use in the estimation of relative humidity. *Geochimica et Cosmochimica Acta* 58(16):3439–3449.

43. Thornthwaite CW (1948) An approach toward a rational classification of climate. *The Geographical Review* 38:55–94.

44. Lehmann CER, Archibald S, Hoffmann WA, Bond WJ (2011) Deciphering the

distribution of the savanna biome. *New Phytologist* 191:197–209.

45. Kohn MJ (1996) Predicting animal $\delta^{18}O$: Accounting for diet and physiological adaptation. *Geochimica et Cosmochimica Acta* 60(23):4811–4829.

46. Levin NE, Zipser E, Cerling TE (2009) Isotopic composition of waters from Ethiopia and Kenya: Insights into moisture sources for eastern Africa. *Journal of Geophysical Research* 114:2–13.

47. White TD, et al. (2009) Macrovertebrate paleontology and the Pliocene habitat of *Ardipithecus ramidus*. *Science* 326:87–93.

48. Leakey MG, Feibel CS, McDougall I, Walker A (1995) New four-million-year-old hominid species from Kanapoi and Allia Bay, Kenya. *Nature* 376(6541):565–571.

49. Cerling TE, et al. (2011) Woody cover and hominin environments in the past 6 million years. *Nature* 476(7358):51–56.

50. Plummer TW, et al. (2009) Oldest evidence of tool making hominins in a grassland-dominated ecosystem. *PLoS ONE* 4(9):e7199.

51. Brown FH, McDougall I, Fleagle JG (2012) Correlation of the KHS Tuff of the Kibish Formation to volcanic ash layers at other sites, and the age of early Homo sapiens (Omo I and Omo II). *Journal of Human Evolution* 63(4):577–585.

52. Staver AC, Archibald S, Levin S (2011) Tree cover in sub-Saharan Africa: Rainfall and fire constrain forest and savanna as alternative stable states. *Ecology* 92:1063–1072.

53. Lehmann CER, et al. (2014) Savanna Vegetation-Fire-Climate Relationships Differ Among Continents. *Science* 343(6170):548–552.

54. Oliveras I, Malhi Y (2016) Many shades of green: the dynamic tropical forest–savannah transition zones. *Philosophical Transactions of the Royal Society B: Biological Sciences* 371(1703):20150308.

55. Sankaran M, et al. (2005) Determinants of woody cover in African savannas. *Nature* 438(7069):846–849.

56. Guan K, et al. (2014) Terrestrial hydrological controls on land surface phenology of African savannas and woodlands. *Journal of Geophysical Research: Biogeosciences* 119(8):1652–1669.

57. Hirota M, Holmgren M, Van Nes EH, Scheffer M (2011) Global Resilience of Tropical Forest and Savanna to Critical Transitions. *Science* 334(6053):232–235.

58. Passey BH, et al. (2010) High-temperature environments of human evolution in East Africa based on bond ordering in paleosol carbonates. *Proceedings of the National Academy of Sciences* 107(25):11245–11249.

59. Lüdecke T, et al. (2016) Persistent C_3 vegetation accompanied Plio-Pleistocene hominin evolution in the Malawi Rift (Chiwondo Beds, Malawi). *Journal of Human Evolution* 90:163–175.

60. Bonnefille R, Potts R, Chalié F, Jolly D, Peyron O (2004) High-resolution vegetation and climate change associated with Pliocene *Australopithecus afarensis*. *Proceedings of the National Academy of Sciences* 101(33):12125–12129.

61. Quinn RL, et al. (2013) Pedogenic carbonate stable isotopic evidence for wooded habitat preference of early Pleistocene tool makers in the Turkana Basin. *Journal of Human Evolution* 65:65–78.

62. Lepre CJ, et al. (2011) An earlier origin for the Acheulian. *Nature* 477(7362):82–85.

63. Harris JM, Brown FH, Leakey MG, Walker AC, Leakey RE (1988) Pliocene and Pleistocene hominid-bearing sites from west of Lake Turkana, Kenya. *Science* 239:27–33.

64. Robinson JR, Rowan J, Faith JT, Fleagle JG (2016) Paleoenvironmental change in the late middle Pleistocene – Holocene kibish formation, Southern Ethiopia: Evidence from ungulate isotopic ecology. *Palaeogeography Palaeoclimatology Palaeoecology*:1–46.

65. Brown FH, Fuller CR (2008) Stratigraphy and tephra of the Kibish Formation, southwestern Ethiopia. *Journal of Human Evolution* 55(3):366–403.

Figure Legends

Figure 1. Map of study area. (A), Detailed map of fossil exposures (red areas) and sites (red circles) and drainages associated with the Nachukui Formation, west of Lake Turkana**.** (B) Fossil collection sites and formations in the Omo-Turkana Basin. (C) Map of Africa with sampling locations for modern teeth and meteoric water (white circles) and fossil sites (red circles).

Figure 2. Isotopic enrichment between enamel and meteoric water ($\varepsilon_{enamel\text{-}mw}$) among eastern and central African herbivores. (A), evaporation insensitive (EI) taxa, (B), evaporation sensitive (ES) taxa, and (C), other bovid, equid, and suids. Error bars represent propagated standard error of $\varepsilon_{enamel\text{-}mw}$ values. Data compiled in Datasets S1 and S2.

Figure 3. Isotopic enrichment ($\varepsilon_{ES\text{-}EI}$) between modern ES and EI taxa. $\varepsilon_{ES\text{-}EI}$ calculated using mean $\delta^{18}O_{enamel}$ values of sampled ES taxa (rows) and EI taxa (columns) from eastern and central Africa. Dashed lines show significant WD-$\varepsilon_{ES\text{-}EI}$ regressions (see Table S4). Error bars represent propagated standard error of $\varepsilon_{ES\text{-}EI}$. Calculated from values given in Dataset S2.

Figure 4. Compilation of data indicating aspects of climate and ecology over the past 5 million years in the Omo-Turkana Basin. (A) Paleoaridity estimates, with error bars indicating age uncertainty and propagated standard error of mean water deficit estimates using all available combinations of ES and EI taxa (see Table S3). (B) Deep lake intervals (62). (C) Paleosol carbonate clumped-isotope temperatures (63). (D) Carbon isotope values of pedogenic

carbonates ($\delta^{13}C_{pc}$) (64). There is a trend towards increasing $\delta^{13}C$ values over time ($p < 0.0001$, $r^2 = 0.2442$). (E) Percent C_4 grazers among Artiodactyla-Perissodactyla-Proboscidea (APP). There is a trend towards including proportion of C_4 grazers over time ($p < 0.001$, $r^2 = 0.7391$). (F) A schematic timeline showing appearances of major hominin behaviors and taxa in eastern Africa (see note in SI).

Figure 5. WD (mm/y) and the proportion of C_4 grazers, C_3-C_4 mixed feeders, and C_3 browsers calculated using the average $\delta^{13}C$ value of each taxon. (A) Modern collections in eastern and central Africa. (B) Fossil collections in eastern Africa. Modern data (51, 65) and fossil data are summarized in SI Appendix, Table S5 and compiled in SI Appendix, Dataset S4.

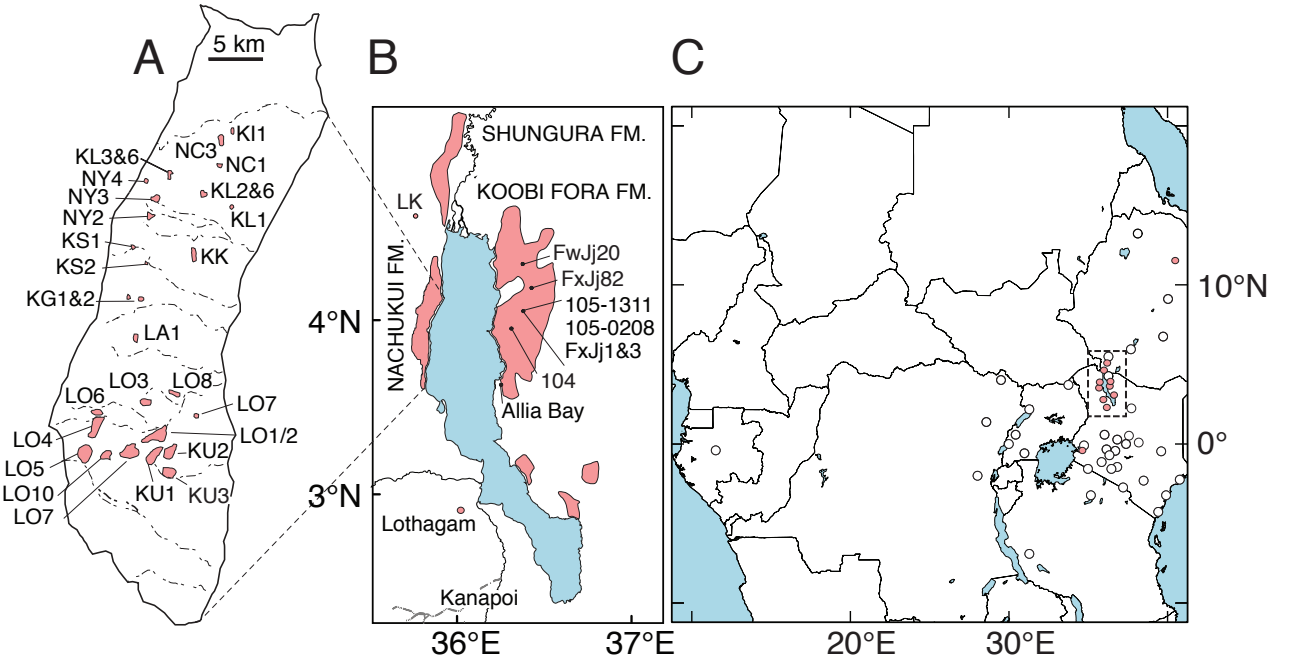
A
5 km
KI1
NC3
NC1
KL3&6
NY4
KL2&6
NY3
NY2
KL1
KS1
KK
KS2
KG1&2
LA1
LO3
LO8
LO6
LO7
LO4
LO1/2
KU2
LO5
LO10
KU1
KU3
LO7
B
SHUNGURA FM.
KOOBI FORA FM.
LK
NACHUKUI FM.
FwJj20
FxJj82
105-1311
105-0208
FxJj1&3
104
Allia Bay
4°N
3°N
Lothagam
Kanapoi
36°E
37°E
C
10°N
0°
20°E
30°E

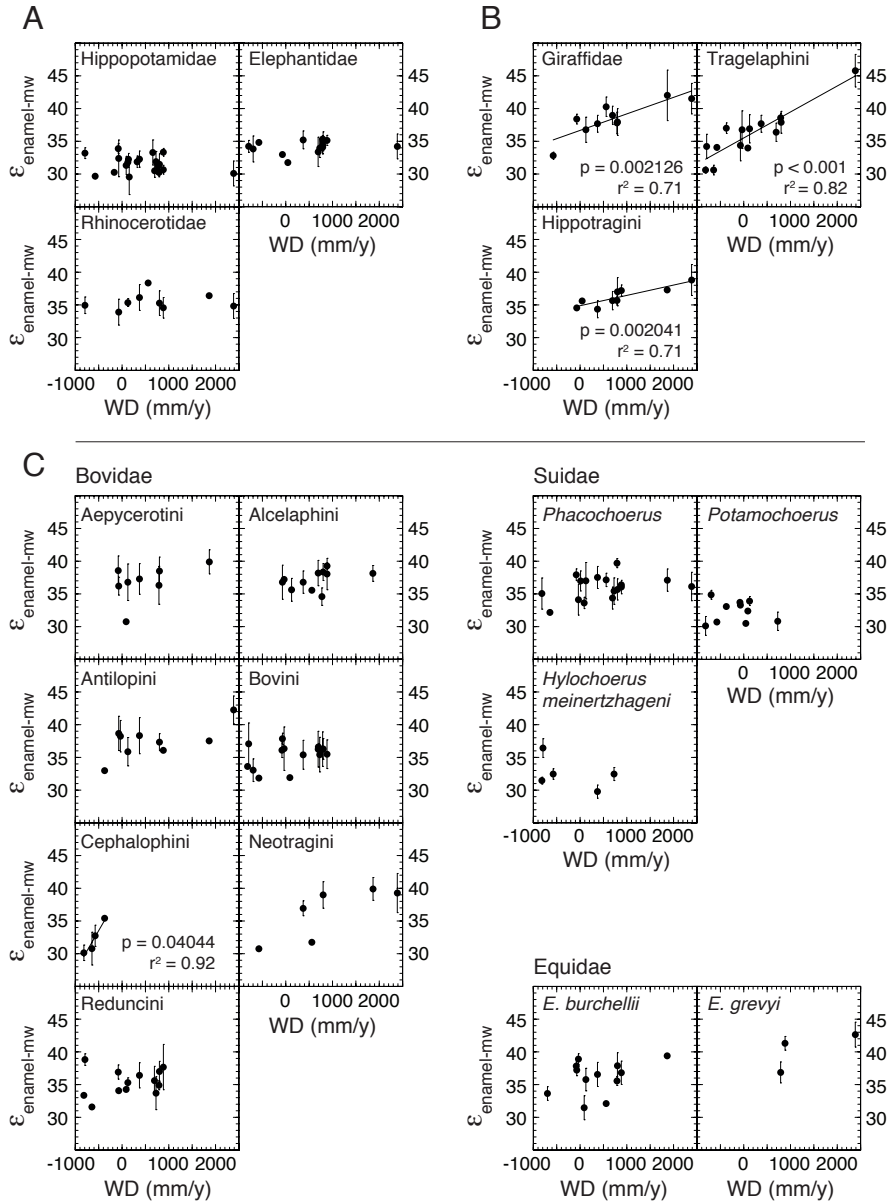
A
Hippopotamidae
Elephantidae
Rhinocerotidae
B
Giraffidae
p = 0.002126
r² = 0.71
Tragelaphini
p < 0.001
r² = 0.82
Hippotragini
p = 0.002041
r² = 0.71
C
Bovidae
Aepycerotini
Alcelaphini
Antilopini
Bovini
Cephalophini
p = 0.04044
r² = 0.92
Neotragini
Reduncini
Suidae
Phacochoerus
Potamochoerus
Hylochoerus meinertzhageni
Equidae
E. burchellii
E. grevyi
εenamel-mw
WD (mm/y)

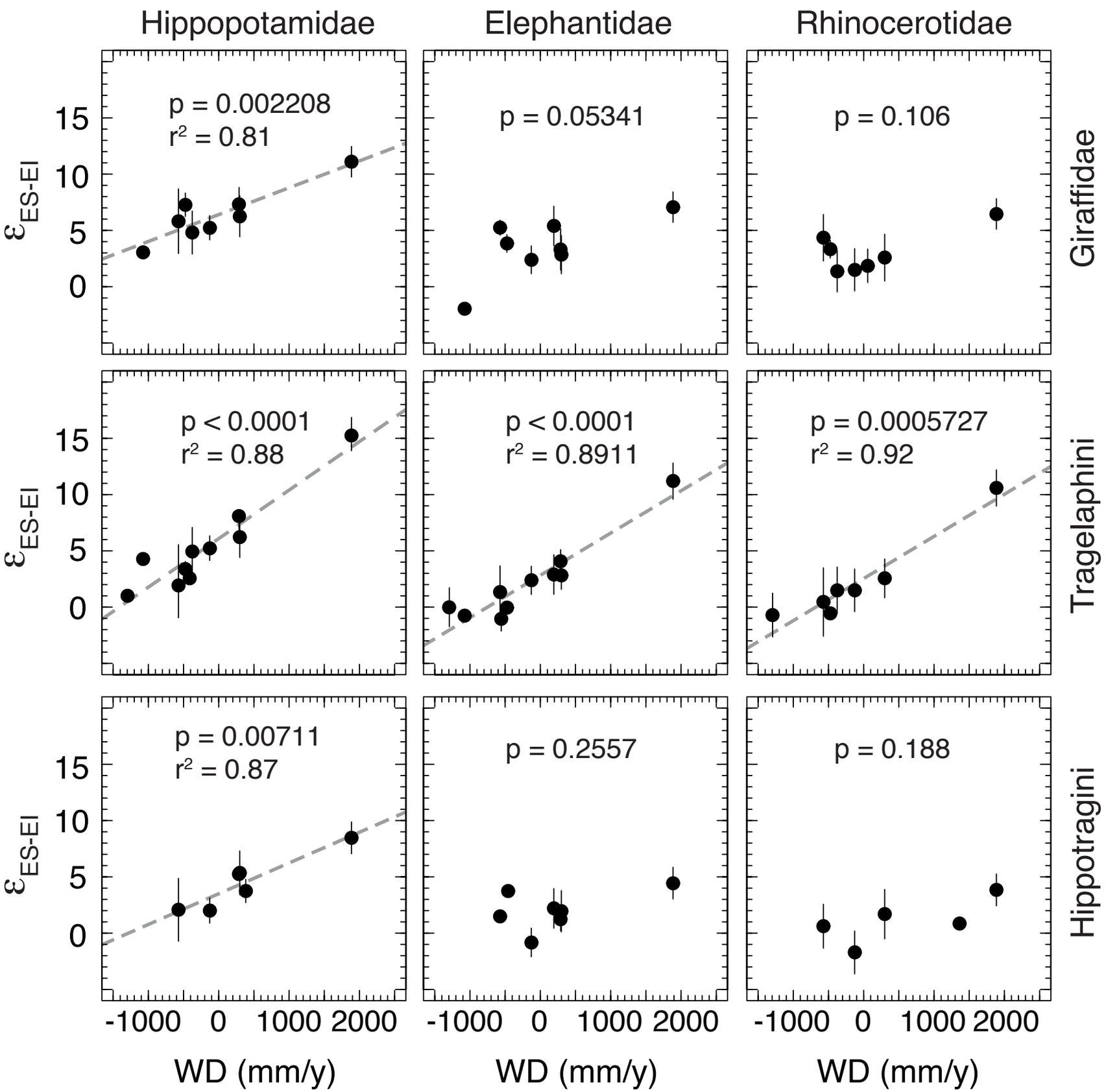
Hippopotamidae
Elephantidae
Rhinocerotidae
Giraffidae
Tragelaphini
Hippotragini
p = 0.002208
r² = 0.81
p = 0.05341
p = 0.106
p < 0.0001
r² = 0.88
p < 0.0001
r² = 0.8911
p = 0.0005727
r² = 0.92
p = 0.00711
r² = 0.87
p = 0.2557
p = 0.188
ε ES-EI
WD (mm/y)
-1000
0
1000
2000
15
10
5
0

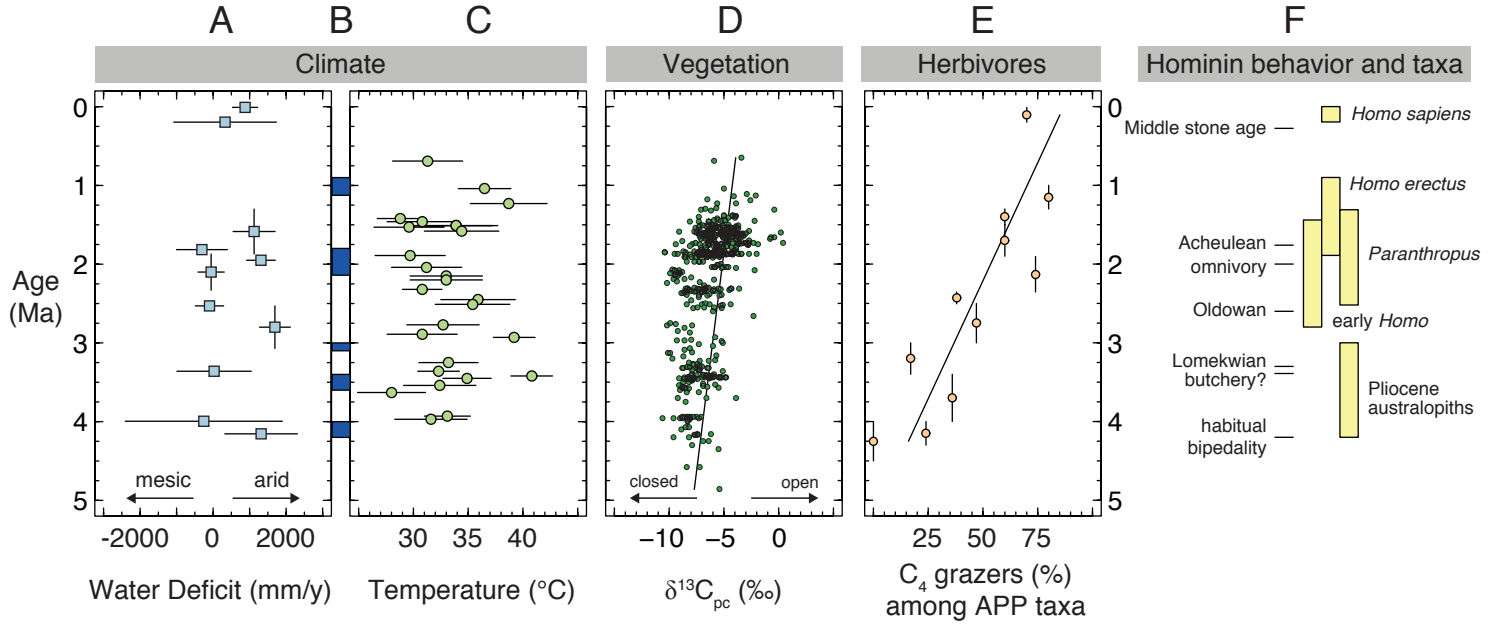
A
B
C
D
E
F
Climate
Vegetation
Herbivores
Hominin behavior and taxa
Age (Ma)
0
1
2
3
4
5
mesic
arid
-2000
0
2000
Water Deficit (mm/y)
30
35
40
Temperature (°C)
closed
open
−10
−5
0
δ13Cpc (‰)
25
50
75
C4 grazers (%) among APP taxa
Middle stone age
Homo sapiens
Homo erectus
Acheulean
omnivory
Paranthropus
Oldowan
early Homo
Lomekwian
butchery?
Pliocene
australopiths
habitual
bipedality

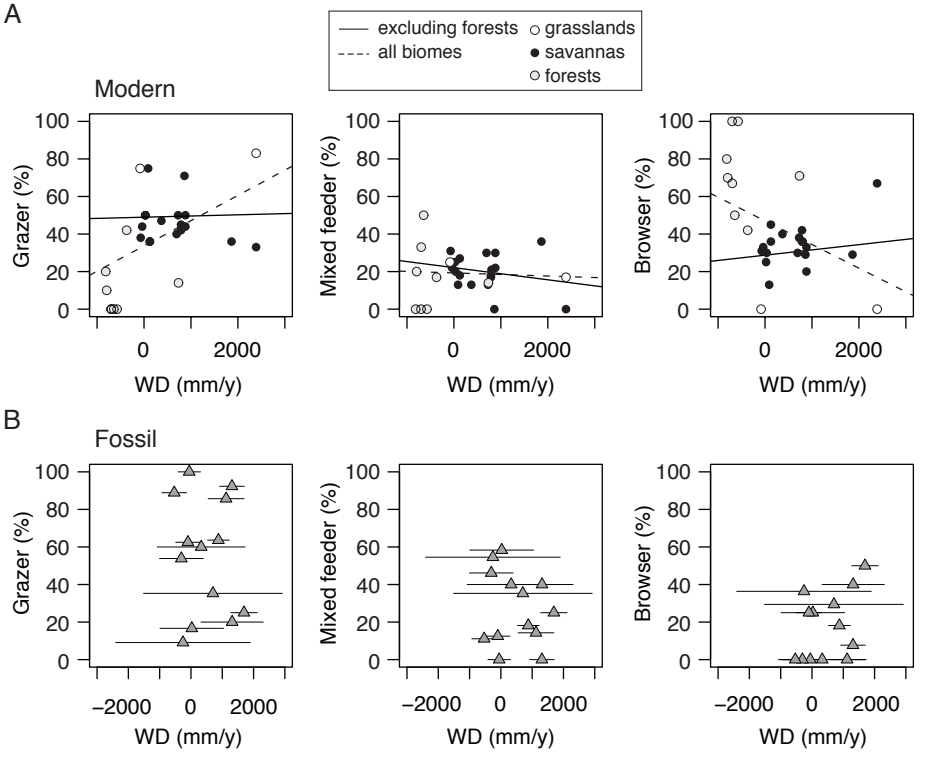
A
excluding forests
all biomes
grasslands
savannas
forests
Modern
Grazer (%)
Mixed feeder (%)
Browser (%)
WD (mm/y)
B
Fossil
Grazer (%)
Mixed feeder (%)
Browser (%)
WD (mm/y)

SUPPLEMENTAL INFORMATION APPENDIX

Index:

1. Methods
    1. Isotopic analysis
    2. Statistics
2. Criteria for the application of the aridity index
    1. Choice of taxa
    2. Geological context – deposition rate
    3. Geological context – sedimentary environments
    4. Diagenesis
    5. Sample size
3. Water deficit calculations
4. Leaf water and cellulose model
5. Body water model
6. Materials
7. Geological context
    1. Fossil collections in the Omo-Turkana Basin
    2. Other fossil collections
8. Note on Fig. 4
9. Datasets
10. References
11. Tables
12. Figures

1. Methods.

1.1. Isotopic analysis. Stable oxygen isotope ratios $^{18}O/^{16}O$ are reported in permil (‰) notation:

$$\delta^{18}O = \left(\frac{R_{sample}}{R_{standard}} - 1\right) * 1000 \quad (1)$$

where R is $^{18}O/^{16}O$. Isotopic ratios are reported using VSMOW (standard mean ocean water) and VPDB (Vienna Pee Dee Belemnite) standards for waters (meteoric, body) and tooth enamel carbonate, respectively. Oxygen isotope ratios can be converted to the VPDB scale from the VSMOW scale using the following relationship (1):

$$\delta^{18}O_{VPDB} = \frac{\delta^{18}O_{VSMOW} - 30.91}{1.03091} \quad (2)$$

The enrichment (ε) between two isotope values, independent of scale, is calculated using the fractionation factor (α) (2). The fractionation factor is

$$\alpha_{A-B} = \frac{R_A}{R_B} = \frac{1000 + \delta_A}{1000 + \delta_B} \quad (3)$$

and isotopic enrichment is

$$\varepsilon^*_{A-B} = (\alpha_{A-B} - 1) * 1000 \quad (4)$$

where A and B refer to any two data groupings and the asterisk indicates that chemical equilibrium is not assumed. Stable oxygen isotopes in tooth enamel carbonate were measured by reacting enamel powder samples with 100% H_3PO_4 at 90 °C and analyzing the resulting CO_2 on a dual inlet isotope ratio mass spectrometer (Finnigan MAT 252). Modern and fossil internal laboratory reference standards that have been reacted at 25 °C and 90 °C were used to correct for temperature-dependent fractionation in oxygen, using $\alpha^*_{90} = 1.00725$ for fossil tooth enamel and $\alpha^*_{90} = 1.00778$ for modern tooth enamel (3). Prior to isotopic analysis, modern and fossil tooth enamel were pretreated using standard procedures to remove organic contaminants (3% H_2O_2) and secondary exogenous carbonates (0.1 M buffered acetic acid) (4, 5).

1.2. Statistics. Statistical analyses were performed in R (6) or following (7). Following previous studies (8, 9), we propagated error in enrichment (ε) values as the square root of the sum of squares of standard deviations. Uncertainty in water deficit estimated in the fossil record using a single ES-EI taxon pair is calculated by propagating uncertainty in enrichment (ε) values, uncertainty in the slope of WD-ε_{ES-EI} regressions, and uncertainty in residuals of WD-ε_{ES-EI} regressions (water deficit variance not explained by the regression). Uncertainty in water deficit calculations in the fossil record using multiple taxon pairs is calculated by further propagating the uncertainty of individual ES-EI taxon pairs.

2. Criteria for application of the aridity index.

2.1. Choice of taxa. Among evaporation insensitive (EI) taxa, the oxygen isotopic enrichment between tooth enamel and meteoric water does not change with water deficit. Among modern Hippopotamidae, Elephantidae, and Rhinocerotidae, $\varepsilon_{enamel-mw}$ values do not vary with water deficit and are relatively invariant (s.e. ≤ 1.3‰), and thus consistently reflect $\delta^{18}O_{mw}$ values (Fig. 2A). Among other evaporation insensitive taxa, $\varepsilon_{enamel-mw}$ values are more variable and/or do not span the full range of modern environments (Fig. 2C). Among both modern and fossil animals, elephantids and rhinocerotids are consistently enriched compared to hippopotamids (Fig. S7), and as previously found for hippopotamids (10) we find no long-term trends ($p > 0.05$) in $\delta^{18}O_{enamel}$ values among hippopotamids, elephantids, and rhinocerotids from paleoaridity

fossil collections in the Omo-Turkana Basin (Fig. S7B). The oxygen isotopic composition of paleosol carbonates is a function of soil temperature and soil water, which in turn reflects meteoric water (11); therefore, paleosol carbonate $\delta^{18}O$ values provide a record of meteoric water in the geologic record independent of mammalian tooth enamel. In contrast to $\delta^{18}O_{enamel}$ records, there is a long-term increase in paleosol carbonate $\delta^{18}O$ values ($p < 0.0001$, $r^2 = 0.2892$) and estimated soil water $\delta^{18}O$ values (paleosol carbonate $\delta^{18}O$ values corrected for temperature) ($p < 0.001$, $r^2 = 0.4602$) (Fig. S7C). These trends do not explain a large amount of variation through time ($r^2 < 0.5$), but nonetheless reflect an apparent shift between 2.0 Ma and 1.0 Ma (12, 13), which is also apparent in hippopotamid $\delta^{18}O_{enamel}$ values (Fig. S7). Increasing paleosol carbonate $\delta^{18}O$ and soil water $\delta^{18}O$ values likely relate to changes in climate, moisture source (atmospheric circulation), and/or basin hydrology (13, 14). We find no relationship ($p > 0.05$) between meteoric water $\delta^{18}O$ and water deficit across modern eastern African environments (Fig. S2A), consistent with previous findings (8), and therefore we do not infer changes in aridity from meteoric water proxies alone. Ultimately, inter-proxy comparisons are complicated by differences in geographic and/or seasonal moisture sources, such that pedogenic carbonate $\delta^{18}O$ values and evaporation insensitive $\delta^{18}O_{enamel}$ values may not always follow the same pattern even if both reflect meteoric waters generally. Thus, while $\delta^{18}O_{enamel}$ values of fossil Hippopotamidae are more similar to $\delta^{18}O$ values in pedogenic carbonates through time (occupying an overlapping range between ca. -8‰ to 2‰), and may more directly reflect meteoric water, hippopotamids, elephantids, and rhinocerotids appear to reflect meteoric water in a consistent manner in modern and fossil systems (Fig. S2C and Fig. S7A). Thus, for fossil applications of the aridity index we assign Hippopotamidae, Elephantidae, and Rhinocerotidae as EI taxa, as identified in modern ecosystems.

Among evaporation sensitive (ES) taxa, the oxygen isotopic enrichment between tooth enamel and meteoric water responds to water deficit. Identifying evaporation sensitive taxa is potentially more problematic, as there is no proxy for the isotopic composition of ^{18}O-enriched paleo-waters independent of mammalian tooth enamel, and no straightforward associations between changes in diet and water use. Identifying ES taxa as those with highest $\delta^{18}O_{enamel}$ values, without an independent measure of aridity, is not an ideal strategy since this criterion could include taxa that consistently have very high $\delta^{18}O_{enamel}$ values due to diet or drinking behavior regardless of changes in aridity. For fossil applications of the aridity index we assign Giraffidae, Hippotragini, and Tragelaphini as ES taxa, as identified in modern ecosystems (Fig. 2 and Fig. S2).

Mean water deficit estimates from each fossil collection calculated using only ES-Hippopotamid taxon pairs are similar to mean WD estimates calculated using all available combinations of ES and EI taxa (mean difference = 415 mm/y), and the standard error of multiple water deficit values is always smaller than total propagated error of overall mean WD (Fig. S4). Further, the combined uncertainty in WD values for multiple ES-EI taxon pairs (mean = 795 mm/y among fossil collections in the Omo-Turkana Basin) is similar to combined uncertainty in WD values using only hippopotamids (mean = 807 mm/y). Total error of ca. 800 mm/y corresponds to ca. 20% of the WD range in modern eastern African environments, sufficient to detect large long-

term trends. Therefore, to accommodate variable taxonomic preservation in the fossil record, and maximize the number of fossil collections for which it is possible to address paleoaridity, we use mean water deficit calculated with multiple WD-$\varepsilon_{ES\text{-}EI}$ regressions ($\varepsilon_{Giraffid\text{-}Hippopotamidae}$, $\varepsilon_{Tragelaphini\text{-}Hippopotamidae}$, $\varepsilon_{Hippotragini\text{-}Hippopotamidae}$, $\varepsilon_{Tragelaphini\text{-}Elephantidae}$, and $\varepsilon_{Tragelaphini\text{-}Rhinocerotidae}$) using all available ES-EI pairs in each fossil collection.

2.2. Geological context – deposition rate. Applications to the fossil record should be limited to assemblages that have been deposited rapidly, to reduce bias introduced by climate variability when comparing $\delta^{18}O_{enamel}$ values of EI and ES taxa. While the absolute age uncertainty of many assemblages can be relatively large, $\varepsilon_{ES\text{-}EI}$ values can be calculated using fossils deposited within a well-constrained stratigraphic interval (such as associations with tuffs or archaeological horizons) or from collections where taphonomic conditions indicate rapid deposition regardless of chronological precision. Despite restricting our paleoaridity sample to fossils collected from discrete and rapidly deposited sedimentary horizons, it is not possible to relate individual paleoaridity estimates to insolation cycling. Thus, we cannot directly address the impact of orbital-scale climate cyclicity and instead restrict our analysis to long-term, secular trends.

2.3. Geological context – sedimentary environments. $\varepsilon_{ES\text{-}EI}$ values should only be calculated for fossil assemblages characterized by consistent depositional settings, which provide an indication of the paleo-waters available to fossil animals. Due to the strong evaporative enrichment of lake water in eastern Africa (15), the application of the aridity index to fossils should be restricted to depositional contexts characterized by flowing water (i.e. fluvial, deltaic) or the absence of water (i.e. aeolian). Although it is not possible to identify specific water sources of animals in the fossil record, we exclude fossils from primarily lacustrine settings to reduce the possibility of including animals that drank from highly evaporated waters.

2.4. Diagenesis. Numerous studies have demonstrated that tooth enamel is resistant to diagenetic alteration during fossilization and preferred for paleontological application over other biogenic tissues (4, 16-19). The carbon and oxygen isotopic composition of carbonate in tooth enamel are susceptible to different diagenetic parameters, and there are no clear relationships between mineralogical, crystallographic, and chemical changes in enamel with isotopic alteration (16, 18, 20-22). Chemical pre-treatment of fossil tooth enamel with buffered 0.1 M acetic acid is commonly used to remove diagenetic carbonates (4, 5, 23), and we restrict our compilation of $\delta^{18}O_{enamel}$ values in fossils to specimens that have been treated using these methods. Diagenesis was monitored by CO_2 yield, since the addition of pure (100%) inorganic carbonates will markedly increase the amount of CO_2 generated per volume compared to the expected range of pristine biological enamel, where carbonate is ca. 3-4% by volume (4, 24, 25). Unlike $\delta^{13}C_{enamel}$ values, there is no simple ecological indicator for preservation of primary biological signals (i.e. retention of expected C_3- and C_4-feeder end-members) in $\delta^{18}O_{enamel}$ values in fossil teeth, and the aridity index does not predict a consistent isotopic separation among particular taxa without prior knowledge of climate. Fortunately, if undetected diagenetic

alteration of both EI and ES taxa results in a consistent isotopic offset, water deficit calculations that reflect relative isotopic spacing among taxa would not be altered. Fossil $\varepsilon_{ES\text{-}EI}$ values (Fig. S8) fall within the range of modern mesic and arid endmembers in the region (Fig. 3), which suggests that significant diagenetic alteration differentially affecting EI or ES taxa (where $\varepsilon_{ES\text{-}EI} < -5$ or > 15) is unlikely.

2.5. Sample size. A power analysis on regressions between $\varepsilon_{ES\text{-}EI}$ and water deficit (Fig. 3), assuming $\alpha = 0.05$ and $(1 - \beta) = 0.2$, demonstrates that 4-7 samples are needed to determine a difference of 1.3‰ (mean standard deviation of $\delta^{18}O_{enamel}$ values of ES and EI taxa for samples >4 to >7). For $\varepsilon_{Giraffid\text{-}Hippo}$, 1.3‰ corresponds to WD precision of 545 mm/y or 17% of the total WD range. For $\varepsilon_{Tragelaphini\text{-}hippo}$ and $\varepsilon_{Hippotragini\text{-}Hippo}$, 1.3‰ corresponds to WD precision of 301 mm/y or 9% of the total WD range. For $\varepsilon_{Tragelaphini\text{-}Eleph}$, 1.3‰ corresponds to WD precision of 346 mm/y or 11% of the total WD range. For $\varepsilon_{Tragelaphini\text{-}Rhino}$, 1.3‰ corresponds to WD precision of 193 mm/y or 6% of the total WD range. Due to inherent limitations of the fossil record, we accept reduced precision associated with small sample size, which can still be used to reconstruct long-term changes in paleoaridity. The level of precision estimated by power analysis (ca. 200-500 mm/y) is higher than precision of WD estimates using all available combinations of ES and EI taxa (average propagated error ±795 mm/y).

3. Water deficit calculations. Water deficit (WD) describes the interactions of energy supply (temperature, sunlight) and water supply (precipitation) on plants. WD is measured as the difference between potential evapotranspiration (PET) and mean annual precipitation (MAP), such that a positive water deficit represents an arid climate and negative water deficit (or surplus) represents a mesic climate. PET is calculated as a function of mean annual temperature (MAT) and latitude using the Thornthwaite method, which is well-suited for estimating water availability of vegetated surfaces (8, 26). Other methods available for estimating PET (e.g. Penman, Class A pan evaporation) are more appropriate for open water surfaces and likely overestimate PET in eastern African terrestrial environments (27-29). We used available rainfall and temperature data to calculate water deficit for each modern locality (see Table S1).

We calculate PET (mm/y) is calculated using the following equation (26):

$$\text{PET} = \sum_{i=1}^{12} 16 \text{ x } K \text{ x } (10 \text{ x } \frac{t}{I})^{a} \quad (5)$$

where t is temperature, I is an annual heat index:

$$I = \sum_{i=1}^{12} (\frac{t}{5})^{1.514} \quad (6)$$

a is a coefficient:

$$a = 6.75 * 10^{-7} * I^3 - 7.71 * 10^{-5} * I^2 + 1.792 * 10^{-2} * I + 0.49239 \quad (7)$$

and K is factor for duration of sunlight each month, which varies by latitude:

$$K = \frac{\frac{h}{12}}{\frac{S_o}{30}} \quad (8)$$

S_o is the number of days in each month and S is the number of sunlight hours on the 15th of each month:

$$S = 24 * \frac{\omega_s}{\pi} \quad (9)$$

where ω_s is the sunset hour angle (radians):

$$\cos^{-1}(-\tan\phi * \tan\delta) \quad (10)$$

ϕ is latitude (radians) and δ is solar declination (radians):

$$\delta = 0.409 * \left(\sin(2 * \pi) * \frac{n}{365}\right) - 1.39 \quad (11)$$

and n is the number of day of year starting from first of January. Previous calculations of PET (8) incorrectly calculated the coefficient a due to 1) substituting monthly heat index values i for annual heat index values I, and 2) inappropriately rounding constant values (Fig. S1). We use mean annual temperature for t rather than monthly temperatures, which were not available from all locations.

4. Leaf water and cellulose model. The oxygen isotopic composition of leaf water at sites of evaporation ($\delta^{18}O_{lw}$) and leaf cellulose ($\delta^{18}O_{lc}$) were calculated using a modified version of the Craig-Gordon evaporative enrichment model where $\delta^{18}O_{MW}$ and relative humidity were available, and expressed as enrichments over measured meteoric (source) water ($\varepsilon_{leaf\text{-}mw}$) (8, 30, 31). Temperature-dependent equilibrium fractionation (α^*) is calculated using the following equation:

$$\alpha^* = \frac{R_L}{R_V} = e^{\left(\frac{a}{T^2} - \frac{b}{T} - c\right)} \quad (12)$$

where e is Euler's number, a = 1137, b = 0.4156, c = 0.0020667, R_L is liquid water isotope ratio ($^{18}O/^{16}O$), R_V is the water vapor isotope ratio, and T is temperature. Kinetic

fractionation factor associated with diffusion from an evaporating surface inside the leaf is estimated as $\alpha_k = 1.032$, and diffusion through a boundary layer is $\alpha_{kb} = 1.021$ (32). $^{18}O/^{16}O$ ratios in leaf water are calculated with the following equation:

$$\delta^{18}O_{lw} = \left(\left(\frac{\alpha * \left[\alpha_k R_S \left(\frac{e_s - e_a}{e_i} \right) + \alpha_{kb} R_S \left(\frac{e_s - e_a}{e_i} \right) R_A \left(\frac{e_a}{e_i} \right) \right]}{R_{SMOW}} \right) - 1 \right) * 1000 \quad (13)$$

where R_{lw} is the isotope ratio of leaf water, R_S is the isotope ratio of the source water, R_A is the isotope ratio of the atmospheric water vapor, R_{SMOW} is the isotope ratio of the standard VSMOW, e_s is the leaf surface vapor pressure, e_i is internal leaf vapor pressure, and e_a is atmospheric vapor pressure. Vapor pressure equations are available elsewhere (33). We assume that $R_S = \delta^{18}O_{MW}$, $R_A = R_S - 9‰$, T = MAT, stomatal conductance = 0.3 mol $m^{-2}s^{-1}$, and boundary later conductance = 1 mol $m^{-2}s^{-1}$ (8, 30). $^{18}O/^{16}O$ ratios in leaf cellulose are calculated with the following equation:

$$\delta^{18}O_{lc} = F * (\delta^{18}O_{lw} + \alpha_c) + (1 - F) * (\delta^{18}O_{lw} + \alpha_s) \quad (14)$$

where F is the fraction of exchange with medium (leaf) water, α_c is heterotrophic fractionation associated with oxygen from xylem water forming cellulose, and α_s is autotrophic fractionation associated with cellulose formation from sucrose. We assume that $F = 0.42$ (30) and that p_x and $p_{ex} = 27$ (34-36).

5. Body water model. The oxygen isotopic composition of mammalian body water reflects oxygen fluxes and isotopic fractionations relative to meteoric water. We use a body water model to predict how oxygen budgets (changes in proportional intake of oxygen sources) of EI and ES taxa respond to increasing aridity. Body water predictions were calculated using the Kohn model (37) developed for African mammals. The model can be expressed using the following mass balance equation:

$$\delta^{18}O_{BW} = \frac{M_{in,air O_2} * \delta^{18}O_{air O_2} + \sum M_{in,\gamma} * \Delta^{18}O_{\gamma-MW} - \sum M_{out,\beta} * \Delta^{18}O_{\beta-BW}}{\sum M_{out,\beta}} + \frac{\sum M_{in,\gamma} * \delta^{18}O_{MW}}{\sum M_{out,\beta}} \quad (15)$$

where $\delta^{18}O_{BW}$ and $\delta^{18}O_{SW}$ and are the oxygen isotopic composition of body and meteoric water, respectively, $M_{in,airO2}$ describes air oxygen input, $\sum M_{in,\gamma}$ describes all other oxygen input components, $\Delta^{18}O_{\gamma\text{-}SW}$ is the fractionation between the oxygen inputs γ and surface water, and $\Delta^{18}O_{\beta\text{-}BW}$ is the fractionation between oxygen outputs β and body water.

Oxygen influxes include air O_2, free water ingested as drinking water (meteoric water) and liquid water in plants (leaf water), and metabolic oxygen derived from bound O_2 in food. The oxygen isotopic composition of atmospheric O_2 and the oxygen isotopic composition of meteoric water ($\delta^{18}O_{mw}$) do not vary with water deficit ($p > 0.05$) (Fig. S2A). We calculated the oxygen isotopic composition of leaf water ($\delta^{18}O_{lw}$) and leaf cellulose ($\delta^{18}O_{lc}$) using a leaf water model, and $\varepsilon_{lw\text{-}mw}$ and $\varepsilon_{lc\text{-}mw}$ increase with water deficit (leaf water: $r^2 = 0.5175$, $p = 0.002501$; leaf cellulose: $r^2 = 0.5169$, $p = 0.002523$) (Fig. S2B).

Oxygen outfluxes include fecal H_2O, urea, urine, nasal H_2O, skin vapor H_2O, oral H_2O, sweat, and CO_2. We use baseline model parameters representative of a mammalian herbivore (37), since precise behavioral and physiological data on each specific species are not available. Changes to model parameters are expressed relative to this baseline. We do not explicitly account for differences in body size, as proportional oxygen influxes and outfluxes do not markedly vary (<10%) across the body mass range encompassed by the meso- and mega-herbivores under study here (38). Additionally, predictions of a generalized model can be more readily extended, with fewer assumptions, to fossil relatives where precise behavioral and physiological parameters are difficult or impossible to measure. Oxygen outputs are invariant, as EI and ES taxa are characterized by a variety of thermoregulatory strategies (water use efficiency, sweating/panting, sensitivity of skin to water vapor loss) (39-46) that have minor effects on body water $\delta^{18}O$ (< ca. 3‰) (37). Predicted body water isotope ratios are expressed as $\varepsilon_{enamel\text{-}mw}$ by converting initial model output $\delta^{18}O_{BW}$ (VSMOW) values to enamel structural carbonate using the apparent fractionation factor (α^*) of 1.0263 and the following relationship (47):

$$\delta^{18}O_{enamel}(\text{VSMOW}) = (1.0263) * (1000 + \delta^{18}O_{BW}(\text{VSMOW}) - 1000). \quad (16)$$

Predicted $\delta^{18}O_{enamel}$ (VSMOW) values are converted to $\delta^{18}O_{enamel}$ (VPDB) values, and expressed as $\varepsilon_{enamel\text{-}mw}$ using mean $\delta^{18}O_{mw}$ (VPDB) for predicted $\delta^{18}O_{enamel}$ (VPDB) and measured $\delta^{18}O_{mw}$ (VPDB) for measured $\delta^{18}O_{enamel}$ (VPDB). Values were converted between VSMOW and VPDB scales using the following equation (1):

$$\delta^{18}O(\text{VSMOW}) = 1.03091 * \delta^{18}O(\text{VPDB}) + 30.91 \quad (17)$$

Oxygen inputs include $\delta^{18}O_{atmO_2}$ (15.1‰), which is based on an estimate of oxygen incorporated in the lungs of terrestrial animals (37, 48), mean $\delta^{18}O_{mw}$ (-2.9‰) (Fig. S2A), and calculated $\delta^{18}O_{lw}$ and $\delta^{18}O_{lc}$ that vary over a water deficit range (-1000 mm/y to +3000 mm/y) encompassing measured $\delta^{18}O_{enamel}$ values (Fig. S2B). We assume the oxygen isotopic composition of leaf cellulose is representative of the isotopic composition of constitutional oxygen in food (37). Therefore, we model body water with linearly increasing aridity assuming isotopically constant meteoric water and atmospheric O_2 (Fig S2A) and linearly increasing enrichment over meteoric water for leaf water and leaf cellulose, representing food water and oxygen, respectively (Fig. S2B).

Using the body water model, we predict the oxygen isotopic enrichment between body water, expressed as equivalent $\delta^{18}O_{enamel}$ values, and meteoric water ($\varepsilon_{enamel\text{-}mw}$) values assuming linear change in oxygen budgets relative to baseline model parameters representative of a mammalian herbivore (37). We vary the balance of oxygen influxes with increasing water deficit to generate three alternative models each for EI and ES taxa, as well as a static oxygen budget where body water is only affected by changes in the isotopic composition of oxygen inputs.

The distribution of modern water-dependent EI taxa is restricted to areas near drinking water sources in arid environments (49-52) and the moisture content of leaf water in trees and grasses declines with increasing aridity (53-55). We model changes to the oxygen budgets of EI taxa with increasing water deficit driven by a balance between decreasing influx of leaf water (100% to 50% relative to mammalian herbivore baseline) and increasing influx of drinking water (Fig. S2C). Each model describes a balance of increasing proportional drinking water influx and different food O_2 baselines, including (EI model 1) food O_2 at 100% relative to baseline, (EI model 2) food O_2 at 200% relative to baseline, and (EI model 3) food O_2 at 300% relative to baseline. Positive offsets in $\varepsilon_{enamel\text{-}mw}$ across EI taxa may relate to dietary differences associated with the degree of water dependence.

The spatial distribution of water-independent ES taxa, which can survive without drinking water, is not related to the availability of surface water sources (49-52). Additionally, eastern African water-independent ruminants increase food intake when exposed to dehydration and heat stress (46). Therefore, we model changes to the oxygen budgets of ES taxa by decreasing proportional influx of drinking water with increasing water deficit (Fig. S2D). Varying slope in WD-$\varepsilon_{enamel\text{-}mw}$ relationships are modeled with different combinations of variable oxygen influxes, including (ES model 1) all oxygen influxes vary, (ES model 2) only food water influx varies, and (ES model 3) only food O_2 influx varies (Fig. S2D).

6. Materials. The oxygen isotopic composition of meteoric water was determined using published $\delta^{18}O$ values of water samples (n = 161) collected from minimally evaporated sources (i.e. springs, boreholes, streams, rivers) (see Appendix 1). Modern mammalian tooth enamel was sampled from existing skeletal collections as well as field surveys, primarily in protected areas (national parks and reserves), with additional modern $\delta^{18}O_{enamel}$ values compiled from the literature (see Appendix 2). This $\delta^{18}O_{enamel}$ compilation is comparable to a previously published compilation of African mammal $\delta^{13}C_{enamel}$ values (56), although animals known or suspected to drink primarily from evaporated water sources (i.e. lakes) were excluded.

In this study, we present $\delta^{18}O_{enamel}$ values from fossil specimens collected during survey, excavation, and taphonomic study in the Turkana Basin (see Appendix 3). We evaluate paleoaridity using a compilation of new and previously published $\delta^{18}O_{enamel}$ values using teeth from paleontological and archaeological collections that meet criteria for application of the aridity index and are associated with evidence for hominin morphology and behavior. We only calculate $\varepsilon_{ES\text{-}EI}$ values in the fossil record using

$\delta^{18}O_{enamel}$ values generated using the same laboratory. We include fossil collections from the Omo-Turkana Basin (n = 11), Afar (n = 1), and southern Kenya (n = 1) that range in age from ca. 4.4 Ma to 0.01 Ma.

Some studies suggest that mammalian first molars have higher $\delta^{18}O_{enamel}$ values due to the influence of milk, which is thought to have higher $\delta^{18}O$ values compared to drinking water assuming drinking water reflects unevaporated meteoric water (lower $\delta^{18}O$) and milk reflects body water (higher $\delta^{18}O$) (57-59). However, observations of oxygen isotopic variation among various mammals do not clearly indicate a consistent difference; in some cases first molar $\delta^{18}O_{enamel}$ values are higher compared to later forming teeth, and in other cases $\delta^{18}O_{enamel}$ values are lower (60-63). Nonetheless, to reduce this possible source of error first molars and deciduous teeth were avoided when possible.

We restrict our analysis of the long-term history of aridity to fossil collections from the Omo-Turkana Basin, which are well-dated by direct $^{40}Ar/^{39}Ar$ dating of tuffs and geochemical tuff correlations among strata in the Koobi Fora, Nachukui, and Shungura Formations (Fig. 1, Fig. S3) (64). We include fossils collected in strata dated to the early Pliocene (Kanapoi Fm. and the upper Lonyumun Mb., Koobi Fora Fm.), mid-Pliocene (lower Lomekwi Mb., Nachukui Fm.), late Pliocene (upper Lomekwi Mb., Nachukui Fm.), early Pleistocene (upper Burgi Mb., Koobi Fora Fm. and Kaito Mb., Nachukui Fm.), late Middle Pleistocene (Kibish Fm. Mb. 1), and late Pleistocene-Holocene (Kibish Fm. Mb. 4) (64-68). We also investigate the long-term history of the oxygen isotopic composition of meteoric water in the Omo-Turkana Basin using a compilation of $\delta^{18}O_{enamel}$ values (n = 261) from evaporation insensitive taxa (hippopotamids, elephantids, rhinocerotids), which includes fossil collections unsuitable for calculating the aridity index (due to inadequate chronostratigraphic context or taxonomic preservation).

Previously published $\delta^{18}O_{enamel}$ values from fossil collections outside the Omo-Turkana Basin include teeth from early Pliocene sediments at Aramis, Afar region, Ethiopia (Lower Aramis Mb., Sagantole Fm.) (69) and early Pleistocene sediments at Kanjera South, Homa Peninsula, southwestern Kenya (Southern Mb., Kanjera Fm.) (70).

The geological context of fossil collections included in this study are described below. Additionally, $\delta^{18}O_{enamel}$ values, location, stratigraphic position, depositional setting, and estimated age of fossil teeth are available in Appendix 3.

7. Geological context

7.1. Fossil collections in the Omo-Turkana Basin. Location of Formations and fossil sites are illustrated in Fig. 1. The major chronologic and tephrostratigraphic levels in the Kanapoi, Nachukui, Koobi Fora, and Kibish Formations, as well as stratigraphic position of fossil collections included in this study (Fig. S3) are based on previous geological research (64, 66, 68, 71-74) except when noted below.

Fossils from the Kanapoi Formation are associated with a paleosol directly above the lower pumiceous tuff (4.2 Ma) and a channel complex below the Kanapoi Tuff (4.11 Ma), which represent the same fluvial system of the ancestral Kerio River (64, 74-77).

Fossils from the Nachukui Formation include teeth collected from the lower Lomekwi member localities Lomewki 4 and 5 (LO4/5), which include pebble conglomerates representing ephemeral stream deposition immediately above the Tulu Bor Tuff (3.44 Ma) (64, 66, 79). Fossils from the upper Lomekwi Member were collected from a stratigraphically narrow section at fossil collection locality Kangatukuseo 1 (KU1), stratigraphically below the Lokalalei Tuff (2.53 Ma) and above the Hasuma Tuff (3.07 Ma) (64, 66, 73). Fossils that span the boundary between the upper Lomekwi Member and the Lokalaei Member, defined by the Lokalalei Tuff, were collected at localities Kangatukuseo 2 and 3 (KU2/3), where fossils are found just below and above the Lokalalei Tuff (2.53 Ma) (64, 66, 73). Fossils from the Kaito Member include teeth from fossil localities Kalochoro 3 and 6 (KL3/6), which both lie above the level of the KBS Tuff (1.87 Ma) and approximately 30 m below the level of the Nariokotome Tuffs (1.30 Ma) exposed in the uppermost part of the Nachukui drainage, and Naiyena Engol 2 and 3 (NY2/3), which both lie above the KBS Tuff and below the level of the Okote Tuff at approximately the same stratigraphic level as KL3/6 (64, 66, 81). Fossils from the upper Kaito Member include teeth collected from the archaeological site Kokiselei 1 (KS1), which lies between the KBS Tuff (1.87 Ma) and KS4 (1.76 Ma) (82). Sediments at Kokiselei 2 (KS2) were originally described as below the Okote Tuff within the Kaitio Member (66), but this is not correct. The site lies below the KBS Tuff (1.87 Ma), exposed to the southwest, but above the Kalochoro Tuff (2.33 Ma) within the Kalochoro Member.

Fossils from the Koobi Fora Formation include teeth collected from the upper Lonyumum Member at the Allia Bay 261-1 excavation site, from a sandy horizon 5 m below the Moiti Tuff (3.97 Ma) representing floodplain deposition of the ancestral Omo River (64, 75, 78). Fossils from the upper Burgi Member were collected at the FwJj20 archaeological site in Area 41, which lies 14 m below the KBS Tuff and is dated to 1.95 Ma (80).

We use previously published $\delta^{18}O_{enamel}$ values from fossils collected in Member 1 and Member 4 of the Kibish Formation (83). Sediments in the Kibish Formation are primarily deltaic, associated with high stands of nearby ancient Lake Turkana (84, 85). Member 1 is the oldest member, dated by the Nakaa'kire Tuff (0.196 Ma) (84, 86), and Member 4 is the youngest, dated to ca. 13-4 Ka by radiocarbon dating of mollusks (85). Based on radiometric dates, association with high lake levels, and estimated deposition time based on sediment-flux calculations, fossils from Member 1 (4,800 yr deposition interval) and Member 4 (7,200 yr deposition interval) were likely deposited rapidly with minimal climate-averaging within sapropel formation intervals S7 and S1, respectively (84, 85).

We also present $\delta^{18}O_{enamel}$ values from other fossil collections that could not be used to calculate water deficit because the necessary combinations of taxa were not available.

Fossils from the Nachukui Formation include teeth collected from the upper Kataboi Member locality Lomekwi 6 (LO6), from a horizon 8 m below the Tulu Bor Tuff (3.44 Ma) (64). Additional fossils from the upper Kataboi Member were collected at locality Loruth Kaado 1 (LK1) from a horizon beneath the Tulu Bor Tuff (66). We use the date of the underlying Lokochot Tuff (3.6 Ma) (64) as the lower boundary for the age

of this collection. Fossils from the middle Lomewki Member were collected at localities Lomewki 9 and 10 (LO9/10), between the Allia and Hasuma Tuffs (3.07 Ma) (64). The Allia Tuff is undated, so we use the date of the underlying Toroto Tuff (3.31 Ma) (64) as the lower boundary for the age of this collection. Fossils that span the boundary between the upper Lomekwi Member and the Lokalaei Member, defined by the Lokalalei Tuff, were collected at localities Lomewki 1 and 2 (LO1/2), where fossils are found just below and above the Lokalalei Tuff (2.53 Ma) (64). Fossils from the Lokalalei Member were collected from Lomewki 8 (LO8), between the Lokalalei and Kalochoro Tuffs (2.33 Ma) (64). Fossils from the Kalochoro Member were collected from Kalokodo (KK), below the KBS Tuff (1.87 Ma) (64). Additional fossils from the Kalochoro Member were collected from Lomekwi 3 (LO3). Here we revise the previously published (66) incorrect stratigraphic position for LO3 as lying below the Lokalalei Tuff and thus having an age of > 2.53 Ma. This site is situated in a small tributary to Lomekwi, entering the larger stream from the north, and most of the area of the site is located east of a fault that trends N30ºE and dips 75ºNW. Strata are downdropped on the west, and drag such that beds in the hanging wall dip 20º to the west immediately in the vicinity of the fault. Strata to the west of this fault are thus younger than those on the east, which includes most of the vertebrate fossil site LO3. At LO3, the beds are nearly flat lying, and the Kokiselei Tuff (ca. 2.4 Ma), and the Kalochoro Tuff both lie below the level of LO3. It is likely that a currently unnamed correlate of Tuff G of the Shungura Formation (2.27 Ma) (64) lies below the fossil site as well. Lacustrine strata of the Lorenyang lake sequence do not appear at the site, but are well exposed at Kangaki, ~8.5 km due north of LO3, where the Kangaki Tuff has been dated at 2.06 Ma (64). The site includes a very distinctive tuff (maximum thickness 2 m) in a channel that has not yet been identified in any other section in the Omo-Turkana Basin; even locally it does not extend far beyond LO3. Thus, we believe that LO3 is confined by the Kangaki Tuff (2.06 Ma) and the correlate of Tuff G (2.27 Ma). Fossils from the Kaitio Member were collected from Loruth Kaado 4 (LK4), which include sediments between the Malbe Tuff (1.84 Ma) and the Morutot Tuff (1.61 Ma) (64). Fossils from the Natoo Member were collected from fossil localities Kalochoro 1 (KL1), which lies in the north arm of Kalochoro above the level of the Ebei Tuff (1.48 Ma) and below the level of the Lower Nariokotome Tuff (1.30 Ma) (64), and Kaito (KI2), which was previously described as above the Okote Tuff (66), but is above the level of the Etirr Tuff, dated to 1.43 Ma by correlation to a directly dated tuff at Konso, Ethiopia (87), and below the level of the Lower Nariokotome Tuff. Fossils from the Nariokotome Member were collected from fossil localities Nachukui 1, 2, and 4 (NC1/2/4).

Fossils from the Koobi Fora Formation include teeth collected from the KBS Member taphonomic collection localities in Areas 104 and 105 on the eastern side of Lake Turkana. Fossils from Area 104 are from a channel sand deposit in the KBS member. Fossils from Area 105 include specimens from collection area 105-1311, located in a 4.5 m thick coarse sandstone horizon deposited in a fluvial channel that cuts into the KBS Tuff, and from archaeological site FxJj1, which lies in the KBS Tuff.

We also use other previously published $\delta^{18}O_{enamel}$ values from fossils of EI taxa collected in the Omo Mursi Formation (88), the Shungura Formation (89), the Nachukui

Formation (Apak, Lokochot, Kaiyumung Members) (90), and the Koobi Fora Formation (Upper Lonyumun, Tulu Bor, upper Burgi, KBS, and Okote Members) (10, 90, 91), which do not meet the criteria for application but are useful for assessing long-term trends in $\delta^{18}O_{enamel}$ values of individual taxa.

7.2. Other fossil collections. We use previously published $\delta^{18}O_{enamel}$ values from fossils collected in the Lower Aramis Member of the Sagantole Formation, primarily from localities ARA-VP-1 and 6 with additional fossils from ARA-VP-7 and 17, KUS-VP-2, and SAG-VP-7, in sediments between the Gàala ("Camel") Tuff Complex (GATC) (4.419 Ma) and the Daam Aatu ("Baboon") Basaltic Tuff (DABT) (4.416 Ma) representing alluvial floodplain deposition (92, 93). Based on statistically indistinguishable tephra $^{40}Ar/^{39}Ar$ ages and inferred environmental and evolutionary stability the Lower Aramis Member is estimated to have accumulating over hundreds to thousands of years (92).

We use previously published $\delta^{18}O_{enamel}$ values from fossils collected in the Southern Member of the Kanjera Formation were collected from excavation and survey from the second lowermost bed, KS-2 (70). KS-2 is a well-sorted fluvial silt to fine pebbly sand deposited by sheet wash and shallow, ephemeral streams. Diffuse conglomerate lenses are indicative of short intervals of higher energy flow (70, 94). KS-2 is highly fossiliferous, and includes abundant Oldowan lithics and cut-marked bone (95-98). Hominins were the primary agent of deposition in the non-conglomeratic sediments, and sedimentology and fine-scale stratigraphy suggests that deposition occurred rapidly over decades to hundreds of years (97, 98). Kanjera South is dated through a combination of biostratigraphy and magnetostratigraphy. The presence of *Deinotherium* sp, *Metridiocheorus andrewsi*, and *Equus* provides an estimated age range of ca. 2.3-1.7 Ma. There is a reversed sequence in Beds KS-1 to KS-3, and normal in Beds KS-4 and KS-5, which is identified as the Olduvai Subchron C2n (1.778-1.945 Ma). Therefore, KS-1 to KS-3 archaeological levels are slightly older than 1.95 Ma, and given the apparent rapidity of deposition we use an estimated age of ca. 2.0 Ma (70, 97).

8. Note on Figure 4. In panel E, we show percent C_4 grazers among Artiodactyla-Perissodactyla-Proboscidea (APP), following (56) and updated to include data from the Omo Mursi Formation (88) and the Kibish Formation (83). Percent C_4 grazer values are calculated using the average $\delta^{13}C$ value of each taxon within a single time interval to identify C_4 grazers (> -1‰), C_3-C_4 mixed feeders (between -8‰ and -1‰), and C_3 browsers (< -8‰) (56).

In panel G, we include a schematic compilation of currently known appearance ages of significant hominin behaviours and taxa. Behaviors include: habitual bipedality in *Australopithecus anamensis* (ca. 4.2-4.1 Ma) (75); possible evidence of butchery from cut-marked bones at Dikika, Ethipia (99); the earliest lithic industry (Lomekian) from Lomekwi, West Turkana, Kenya (100); the appearance of the earliest Oldowan lithics (ca. 2.6 Ma) at Gona (101, 102) (the earliest Oldowan lithics in the Omo-Turkana Basin are documented in the Nachukui Formation ca. 2.34 Ma (103)); earliest evidence for omnivory, based on zooarchaeological studies of Oldowan faunal assemblages indicating

hominin consumption of diverse foods including animal- and plant-based resources at Kanjera South (ca. 2.0 Ma) (97, 104) and terrestrial and aquatic resources in the Koobi Fora Formation of the Omo-Turkana Basin at FwJj 20 (ca. 1.95 Ma) (80, 105); the appearance of Acheulean lithics (ca. 1.76 Ma) in the Nachukui Formation, West Turkana, Kenya and the Konso Formation, southern Ethiopia (82, 106); the appearance of Middle Stone Age lithics in the Gademotta Formation (ca. > 0.276 Ma) (107) (the earliest Middle Stone Age lithics in the Omo-Turkana Basin are documented in the Kibish Formation ca. 0.195 Ma (85, 86, 108)). Age distributions of eastern African hominin taxa (84, 86, 109-112) use the following informal groupings: Pliocene australopiths (including age distribution of specimens assigned to *Australopithecus anamensis*, *Australopithecus afarensis*, *Kenyanthropus platyops*), early *Homo* (including the earliest representatives of the genus and later specimens often assigned to *H. habilis* and *H. rudolfensis*), *Homo erectus* (including specimens often assigned to *H. ergaster*), *Paranthropus* (including specimens assigned to *P. aethiopicus*, *P. boisei*), and *Homo sapiens*.

9. Datasets.

9.1. Dataset 1. A compilation of oxygen isotope data for water samples collected in central and eastern Africa.

9.2. Dataset 2. A compilation of oxygen isotope data for modern herbivore tooth enamel from specimens collected in central and eastern Africa.

9.3. Dataset 3. A compilation of oxygen isotope data for herbivore tooth enamel from fossil collections in eastern Africa meeting criteria for application of the aridity index and used for calculating paleoaridity.

9.4. Dataset 4. A compilation of carbon isotope data for herbivore tooth enamel from fossil collections in the Omo-Turkana Basin meeting criteria for application of the aridity index and used for calculating percent C_4 grazers, C_3-C_4 mixed-feeders, and C_3 browsers.

10. Supplementary Information References.

1. Sharp Z (2007) *Principles of stable isotope geochemistry* (Pearson Education Upper Saddle River, NJ, USA).

2. Craig H (1954) Carbon 13 in plants and the relationships between carbon 13 and carbon 14 variations in nature. *The Journal of Geology* 62:115–149.

3. Passey BH, Cerling TE, Levin NE (2007) Temperature dependence of oxygen isotope acid fractionation for modern and fossil tooth enamels. *Rapid communications in mass spectrometry* 21(17):2853–2859.

4. Koch PL, Tuross N, Fogel ML (1997) The effects of sample treatment and

diagenesis on the isotopic integrity of carbonate in biogenic hydroxylapatite. *Journal of Archaeological Science* 24:417–429.

5. Crowley BE, Wheatley PV (2014) To bleach or not to bleach? Comparing treatment methods for isolating biogenic carbonate. *Chemical Geology* 381:234–242.

6. R: A language and environment for statistical computing (2014) R: A language and environment for statistical computing. *R Foundation for Statistical Computing, Vienna, Austria*:1–105.

7. Sokal RR, Rohlf FJ (2012) *Biometry: the principles and practice of statistics in biological research* (W.H. Freeman and Company, New York).

8. Levin NE, Cerling TE, Passey BH, Harris JM, Ehleringer JR (2006) A stable isotope aridity index for terrestrial environments. *Proceedings of the National Academy of Sciences* 103(30):11201–11205.

9. Passey BH, et al. (2005) Carbon isotope fractionation between diet, breath CO_2, and bioapatite in different mammals. *Journal of Archaeological Science* 32:1459–1470.

10. Harris JM, Cerling TE, Leakey MG, Passey BH (2008) Stable isotope ecology of fossil hippopotamids from the Lake Turkana Basin of East Africa. *Journal of Zoology* 275:323–331.

11. Cerling TE (1984) The stable isotopic composition of modern soil carbonate and its relationship to climate. *Earth and Planetary Science Letters* 71(2):229–240.

12. Passey BH, et al. (2010) High-temperature environments of human evolution in East Africa based on bond ordering in paleosol carbonates. *Proceedings of the National Academy of Sciences* 107(25):11245–11249.

13. Levin NE, Brown FH, Behrensmeyer AK, Bobe R, Cerling TE (2011) Paleosol carbonates from the Omo Group: Isotopic records of local and regional environmental change in East Africa. *Palaeogeography Palaeoclimatology Palaeoecology* 307:75–89.

14. Quade J, Cerling TE, Bowman JR (1989) Systematic variations in the carbon and oxygen isotopic composition of pedogenic carbonate among elevation transects in the southern Great Basin, United States. *GSA Bulletin* 101:464–475.

15. Cerling TE, et al. (2008) Stable isotope ecology of the common hippopotamus. *Journal of Zoology* 276(2):204–212.

16. Wang Y, Cerling TE (1994) A model of fossil tooth and bone diagenesis: implications for paleodiet reconstruction from stable isotopes. *Palaeogeography Palaeoclimatology Palaeoecology* 107(3-4):281–289.

17. Lee-Thorp JA (2008) On Isotopes and Old Bones. *Archaeometry* 50(6):925–950.

18. Zazzo A, Lécuyer C, Mariotti A (2004) Experimentally-controlled carbon and oxygen isotope exchange between bioapatites and water under inorganic and microbially-mediated conditions. *Geochimica et Cosmochimica Acta* 68(1):1–12.

19. Ayliffe LK, Chivas AR, Leakey MG (1994) The retention of primary oxygen isotope compositions of fossil elephant skeletal phopshate. *Geochimica et Cosmochimica Acta* 58:5291–5298.

20. Sponheimer M, Lee-Thorp JA (1999) Alteration of enamel carbonate environments during fossilization. *Journal of Archaeological Science* 26:143–150.

21. Roche D, Ségalen L, Balan E, Balan E, Delattre S (2010) Preservation assessment of Miocene–Pliocene tooth enamel from Tugen Hills (Kenyan Rift Valley) through FTIR, chemical and stable-isotope analyses. *Journal of Archaeological Science* 37(7):1690–1699.

22. Lee-Thorp JA, Sponheimer M (2003) Three case studies used to reassess the reliability of fossil bone and enamel isotope signals for paleodietary studies. *Journal of Anthropological Archaeology* 22(3):208–216.

23. Pellegrini M, Snoeck C (2016) Comparing bioapatite carbonate pre-treatments for isotopic measurements: Part 2—Impact on carbon and oxygen isotope compositions. *Chemical Geology* 420:88–96.

24. Elliott JC (2002) Calcium phosphate biominerals. *Reviews in Mineralogy and Geochemistry* 48(1):427–453.

25. Sakae T, Suzuki K, Kozawa Y (1997) A short review of studies on chemical and physical properties of enamel crystallites. *Tooth Enamel Microstructure*, eds Koeningswald WV, Sander PM (Balkema, Rotterdam), pp 31–39.

26. Thornthwaite CW (1948) An approach toward a rational classification of climate. *The Geographical Review* 38:55–94.

27. Penman HL (1948) Natural evaporation from open water, bare soil and grass. *Proceedings of the Royal Society A* 193:120–145.

28. Dagg M, Blackie JR (1970) Estimates of evaporation in East Africa in relation to

climatological classification. *The Geographical Journal* 136(2):227–234.

29. Cerling TE (1986) A mass-balance approach to basin sedimentation: Constraints on the recent history of the Turkana basin. *Palaeogeography, Palaeoclimatology, Palaeoecology* 54:63–86.

30. Roden JS, Ehleringer JR (1999) Observations of hydrogen and oxygen isotopes in leaf water confirm the Craig-Gordon model under wide-ranging environmental conditions. *Plant Physiology* 120(4):1165–1174.

31. West JB, Sobek A, Ehleringer JR (2008) A Simplified GIS Approach to Modeling Global Leaf Water Isoscapes. *PLoS ONE* 3(6):e2447.

32. Cappa CD, Hendricks MB, DePaolo DJ, Cohen RC (2003) Isotopic fractionation of water during evaporation. *Journal of Geophysical Research: Atmospheres* 108(D16):4525.

33. Ball JT (1987) Calculations related to gas exchange. *Stomatal Function*, eds Zeigler E, Farquhar GD, Cowan IR (Stomatal function, Stanford, CA), pp 445–476.

34. Sternberg LS, DeNiro MJ (1983) Biogeochemical implications of the isotopic equilibrium fractionation factor between the oxygen atoms of acetone and water. *Geochimica et Cosmochimica Acta* 47:2271–2274.

35. Yakir D, DeNiro MJ (1990) Oxygen and Hydrogen Isotope Fractionation during Cellulose Metabolism in *Lemna gibba* L. *Plant Physiology* 93(1):325–332.

36. Luo Y-H, Sternberg LS (1992) Hydrogen and oxygen isotopic fractionation during heterotrophic cellulose synthesis. *J Exp Biol* 43:47–50.

37. Kohn MJ (1996) Predicting animal $\delta^{18}O$: Accounting for diet and physiological adaptation. *Geochimica et Cosmochimica Acta* 60(23):4811–4829.

38. Bryant JD, Froelich PN (1995) A model of oxygen isotope fractionation in body water of large mammals. *Geochimica et Cosmochimica Acta* 59(21):4523–4537.

39. Robertshaw D, Taylor CR (1969) A comparison of sweat gland activity in eight species of East African bovids. *J Physiol (Lond)* 203(1):135–143.

40. Taylor CR, Spinage CA, Lyman CP (1969) Water relations of the waterbuck, an East African antelope. *Am J Physiol* 217(2):630–634.

41. Taylor CR (1970) Dehydration and heat: effects on temperature regulation of East African ungulates. *American Journal of Physiology* 219:1136–1139.

42. Taylor CR, Lyman CP (1972) Heat storage in running antelopes: independence of brain and body temperatures. *Am J Physiol* 222(1):114–117.

43. Maloiy GMO (1973) Water metabolism of East African ruminants in arid and semi-arid regions. *Zeitschrift für Tierzüchtung und Züchtungsbiologie* 90(1-4):219–228.

44. Maloiy GM (1973) The water metabolism of a small East African antelope: the dik-dik. *Proc R Soc Lond, B, Biol Sci* 184(1075):167–178.

45. Woodall PF, Skinner JD (1993) Dimensions of the intestine, diet and faecal water loss in some African antelope. *Journal of Zoology* 229(3):457–471.

46. Maloiy GMO, et al. (2008) Effects of dehydration and heat stress on food intake and dry matter digestibility in East African ruminants. *Comp Biochem Physiol, Part A Mol Integr Physiol* 151(2):185–190.

47. Bryant JD, Koch PL, Froelich PN, Showers WJ, Genna BJ (1996) Oxygen isotope partitioning between phosphate and carbonate in mammalian apatite. *Geochimica et Cosmochimica Acta* 60:5145–5148.

48. Podlesak DW, et al. (2008) Turnover of oxygen and hydrogen isotopes in the body water, CO_2, hair, and enamel of a small mammal. *Geochimica et Cosmochimica Acta* 72(1):19–35.

49. Western D (1975) Water availability and its influence on the structure and dynamics of a savannah large mammal community. *African Journal of Ecology* 13(3-4):265–286.

50. Sitters J, Heitkönig IMA, Holmgren M, Ojwang GSO (2009) Herded cattle and wild grazers partition water but share forage resources during dry years in East African savannas. *Biological Conservation* 142(4):738–750.

51. Ogutu JO, Piepho HP, Reid RS, Rainy ME (2010) Large herbivore responses to water and settlements in savannas. *Ecological Monographs* 80(2):241–266.

52. de Leeuw J, Waweru MN, Okello OO, Maloba M (2001) Distribution and diversity of wildlife in northern Kenya in relation to livestock and permanent water points. *Biological Conservation* 100(3):297–306.

53. Taylor CR (1968) Hygroscopic food: a source of water for desert antelopes? *Nature* 219(5150):181–182.

54. Kay RNB (1997) Responses of African livestock and wild herbivores to drought. *Journal of Arid Environments* 37(4):683–694.

55. Sobrado MA (1986) Aspects of tissue water relations and seasonal changes of leaf water potential components of evergreen and deciduous species coexisting in tropical dry forests. *Oecologia* 68:413–416.

56. Cerling TE, et al. (2015) Dietary changes of large herbivores in the Turkana Basin, Kenya from 4 to 1 Ma. *Proceedings of the National Academy of Sciences* 112(37):11467–11472.

57. Fricke HC, O'Neil JR (1996) Inter-and intra-tooth variation in the oxygen isotope composition of mammalian tooth enamel phosphate: implications for palaeoclimatological and palaeobiological research. *Palaeogeography Palaeoclimatology Palaeoecology* 126(1):91–100.

58. Wright LE, Schwarcz HP (1998) Stable carbon and oxygen isotopes in human tooth enamel: identifying breastfeeding and weaning in prehistory. *American Journal of Physical Anthropology* 106(1):1–18.

59. Franz-Odendaal TA, Lee-Thorp JA, Chinsamy A (2003) Insights from stable light isotopes on enamel defects and weaning in Pliocene herbivores. *Journal of biosciences* 28(6):765–773.

60. Bryant JD, Froelich PN, Showers WJ, Genna BJ (1996) Biologic and climatic signals in the oxygen isotopic composition of Eocene-Oligocene equid enamel phosphate. *Palaeogeography Palaeoclimatology Palaeoecology* 126(1-2):75–89.

61. Bryant JD, Froelich PN, Showers WJ, Genna BJ (1996) A tale of two quarries; biologic and taphonomic signatures in the oxygen isotope composition of tooth enamel phosphate from modern and Miocene equids. *Palaios* 11(4):397.

62. Quinn RL (2015) Influence of Plio-Pleistocene basin hydrology on the Turkana hominin enamel carbonate δ 18 O values. *Journal of Human Evolution* 86:13–31.

63. White C, Longstaffe FJ, Law KR (2004) Exploring the effects of environment, physiology and diet on oxygen isotope ratios in ancient Nubian bones and teeth. *Journal of Archaeological Science* 31(2):233–250.

64. McDougall I, et al. (2012) New single crystal $^{40}Ar/^{39}Ar$ ages improve time scale for deposition of the Omo Group, Omo–Turkana Basin, East Africa. *Journal of the Geological Society* 169(2):213–226.

65. Brown FH, Feibel CS (1986) Revision of lithostratigraphic nomenclature in the Koobi Fora region, Kenya. *Journal of the Geological Society* 143:297–310.

66. Harris JM, Brown FH, Leakey MG, Walker AC, Leakey RE (1988) Pliocene and Pleistocene hominid-bearing sites from west of Lake Turkana, Kenya. *Science*

239:27–33.

67. Brown FH, Feibel CS (1991) Stratigraphy, depositional environments and palaeogeography of the Koobi Fora Formation. *Koobi Fora Research Project, Vol. 3 the Fossil Ungulates Geology, Fossil Artiodactyles, Palaeoenvironments*, ed Harris JM (Oxford), pp 1–30.

68. McDougall I, Brown FH (2008) Geochronology of the pre-KBS Tuff sequence, Omo Group, Turkana Basin. *Journal of the Geological Society* 165(2):549–562.

69. White TD, et al. (2009) *Ardipithecus ramidus* and the paleobiology of early hominids. *Science* 326:75–86.

70. Plummer TW, et al. (2009) Oldest evidence of tool making hominins in a grassland-dominated ecosystem. *PLoS ONE* 4(9):e7199.

71. McDougall I, Feibel CS (1999) Numerical age control for the Miocene-Pliocene succession at Lothagam, a hominoid-bearing sequence in the northern Kenya Rift. *Journal of the Geological Society* 156(4):731–745.

72. McDougall I, Brown FH (2006) Precise $^{40}Ar/^{39}Ar$ geochronology for the upper Koobi Fora Formation, Turkana Basin, northern Kenya. *Journal of the Geological Society* 163:205–220.

73. Feibel CS, Brown FH, McDougall I (1989) Stratigraphic context of fossil hominids from the Omo group deposits: Northern Turkana Basin, Kenya and Ethiopia. *American Journal of Physical Anthropology* 78(4):595–622.

74. Leakey MG, Feibel CS, McDougall I, Ward C, Walker A (1998) New specimens and confirmation of an early age for *Australopithecus anamensis*. *Nature* 393(6680):62–66.

75. Leakey MG, Feibel CS, McDougall I, Walker A (1995) New four-million-year-old hominid species from Kanapoi and Allia Bay, Kenya. *Nature* 376(6541):565–571.

76. Feibel CS (2003) Stratigraphy and Depositional Setting of the Pliocene Kanapoi Formation, Lower Kerio Valley, Kenya. *Geology and Vertebrate Paleontology of the Early Pliocene Site of Kanapoi, Northern Kenya*, eds Harris JM, Leakey MG (Natural History Museum of Los Angeles County), pp 9–20.

77. Harris JM, Leakey MG (2003) *Geology and vertebrate paleontology of the early Pliocene site of Kanapoi, northern Kenya* eds Harris JM, Leakey MG (Natural History Museum of Los Angeles County).

78. Coffing K, Feibel C, Leakey M, Walker A (1994) Four-million-year-Old hominids from East Lake Turkana, Kenya. *American Journal of Physical Anthropology* 93(1):55–65.

79. Leakey MG, et al. (2001) New hominin genus from eastern Africa shows diverse middle Pliocene lineages. *Nature* 410:433–440.

80. Braun DR, et al. (2010) Early hominin diet included diverse terrestrial and aquatic animals 1.95 Ma in East Turkana, Kenya. *Proceedings of the National Academy of Sciences* 107(22):10002–10007.

81. Kibunjia M, Roche H, Brown FH, Leakey RE (1992) Pliocene and Pleistocene archeological sites west of Lake Turkana, Kenya. *Journal of Human Evolution* 23(5):431–438.

82. Lepre CJ, et al. (2011) An earlier origin for the Acheulian. *Nature* 477(7362):82–85.

83. Robinson JR, Rowan J, Faith JT, Fleagle JG (2016) Paleoenvironmental change in the late middle Pleistocene – Holocene kibish formation, Southern Ethiopia: Evidence from ungulate isotopic ecology. *Palaeogeography Palaeoclimatology Palaeoecology*:1–46.

84. Brown FH, McDougall I, Fleagle JG (2012) Correlation of the KHS Tuff of the Kibish Formation to volcanic ash layers at other sites, and the age of early Homo sapiens (Omo I and Omo II). *Journal of Human Evolution* 63(4):577–585.

85. Brown FH, Fuller CR (2008) Stratigraphy and tephra of the Kibish Formation, southwestern Ethiopia. *Journal of Human Evolution* 55(3):366–403.

86. McDougall I, Brown FH, Fleagle JG (2005) Stratigraphic placement and age of modern humans from Kibish, Ethiopia. *Nature* 433(7027):733–736.

87. Brown FH, Haileab B (2006) Sequence of tuffs between the KBS Tuff and the Chari Tuff in the Turkana Basin, Kenya and Ethiopia. *Journal of the Geological Society*.

88. Drapeau MSM, et al. (2014) The Omo Mursi Formation: A window into the East African Pliocene. *Journal of Human Evolution* 75:64–79.

89. Souron A, Balasse M, Boisserie J-R (2012) Intra-tooth isotopic profiles of canines from extant *Hippopotamus amphibius* and late Pliocene hippopotamids (Shungura Formation, Ethiopia): Insights into the seasonality of diet and climate. *Palaeogeography, Palaeoclimatology, Palaeoecology* 342-343:97–110.

90. Cerling TE, Harris JM, Leakey MG (2003) Isotope Paleoecology of the Nawata and Nachukui Formations at Lothagam, Turkana Basin, Kenya. *Lothagam*:605–614.

91. Cerling TE, et al. (2011) Diet of *Paranthropus boisei* in the early Pleistocene of East Africa. *Proceedings of the National Academy of Sciences* 108(23):9337–9341.

92. WoldeGabriel G, et al. (2009) The Geological, Isotopic, Botanical, Invertebrate, and Lower Vertebrate Surroundings of *Ardipithecus ramidus*. *Science* 326(5949):65e1–65e5.

93. White TD, et al. (2009) Macrovertebrate paleontology and the Pliocene habitat of *Ardipithecus ramidus*. *Science* 326:87–93.

94. Ditchfield P, Hicks J, Plummer TW, Bishop LC (1999) Current research on the Late Pliocene and Pleistocene deposits north of Homa Mountain, southwestern Kenya. *Journal of Human Evolution* 36:123–150.

95. Braun DR, et al. (2008) Oldowan behavior and raw material transport: perspectives from the Kanjera Formation. *Journal of Archaeological Science* 35:2329–2345.

96. Braun DR, Plummer TW, Ferraro JV, Ditchfield P, Bishop LC (2009) Raw material quality and Oldowan hominin toolstone preferences: evidence from Kanjera South, Kenya. *Journal of Archaeological Science* 36:1605–1614.

97. Ferraro JV, et al. (2013) Earliest archaeological evidence of persistent hominin carnivory. *PLoS ONE* 8(4):e62174.

98. Plummer TW, Bishop LC, Ditchfield P, Hicks J (1999) Research on late Pliocene Oldowan sites at Kanjera South, Kenya. *Journal of Human Evolution* 36(2):151–170.

99. McPherron SP, et al. (2010) Evidence for stone-tool-assisted consumption of animal tissues before 3.39 million years ago at Dikika, Ethiopia. *Nature* 466(7308):857–860.

100. Harmand S, et al. (2015) 3.3-million-year-old stone tools from Lomekwi 3, West Turkana, Kenya. *Nature* 521(7552):310–315.

101. Semaw S (2000) The World's Oldest Stone Artefacts from Gona, Ethiopia: Their Implications for Understanding Stone Technology and Patterns of Human Evolution Between 2.6-1.5 Million Years Ago. *Journal of Archaeological Science* 27(12):1197–1214.

102. Semaw S, et al. (2003) 2.6-Million-year-old stone tools and associated bones from OGS-6 and OGS-7, Gona, Afar, Ethiopia. *Journal of Human Evolution* 45(2):169–177.

103. Roche H, et al. (1999) Early hominid stone tool production and technical skill 2.34 Myr ago in West Turkana, Kenya. *Nature* 399(6731):57–60.

104. Lemorini C, et al. (2014) Old stones' song: Use-wear experiments and analysis of the Oldowan quartz and quartzite assemblage from Kanjera South (Kenya). *Journal of Human Evolution* 72:10–25.

105. Archer W, Braun DR, Harris JWK, McCoy JT (2014) Early Pleistocene aquatic resource use in the Turkana Basin. *Journal of Human Evolution* 77:74–87.

106. Beyene Y, et al. (2013) The characteristics and chronology of the earliest Acheulean at Konso, Ethiopia. *Proceedings of the National Academy of Sciences* 110(5):1584–1591.

107. Morgan L, Renne PR (2008) Diachronous dawn of Africa's Middle Stone Age: New 40Ar/39Ar ages from the Ethiopian Rift. *Geology* 36(12):967.

108. Shea JJ (2008) The Middle Stone Age archaeology of the Lower Omo Valley Kibish Formation: Excavations, lithic assemblages, and inferred patterns of early Homo sapiens behavior. *Journal of Human Evolution* 55(3):448–485.

109. Wood B, Leakey MG (2011) The Omo-Turkana Basin Fossil Hominins and Their Contribution to Our Understanding of Human Evolution in Africa. *Evolutionary Anthropology Issues News and Reviews* 20(6):264–292.

110. Villmoare B, et al. (2015) Early *Homo* at 2.8 Ma from Ledi-Geraru, Afar, Ethiopia. *Science* 347(6228):1352–1355.

111. Pearson OM, Fleagle JG, Grine FE, Royer DF (2008) Further new hominin fossils from the Kibish Formation, southwestern Ethiopia. *Journal of Human Evolution* 55(3):444–447.

112. Antón SC, Potts R, Aiello LC (2014) Evolution of early *Homo*: An integrated biological perspective. *Science* 345(6192):1236828.

113. Lourens L (2004) Appendix 2: Orbital tuning calibrations and conversions for the Neogene Period. *A Geologic Time Scale*, eds Gradstein FM, Ogg JG, Smith AG, pp 469–484.

114. Wynn J (2004) Influence of Plio-Pleistocene aridification on human evolution: evidence from paleosols of the Turkana Basin, Kenya. *American Journal of*

Physical Anthropology 123(2):106–118.

115. Fernández MH, Vrba ES (2006) Plio-Pleistocene climatic change in the Turkana Basin (East Africa): Evidence from large mammal faunas. *Journal of Human Evolution* 50(6):595–626.

116. Bibi F, Kiessling W (2015) Continuous evolutionary change in Plio-Pleistocene mammals of eastern Africa. *Proceedings of the National Academy of Sciences* 112:10623–10628.

117. Fortelius M, et al. (2016) An ecometric analysis of the fossil mammal record of the Turkana Basin. *Philosophical Transactions of the Royal Society B: Biological Sciences* 371(1698):20150232.

118. Levin NE (2015) Environment and Climate of Early Human Evolution. *The Annual Review of Earth and Planetary Sciences* 43:405–429.

119. East African Meterological Department (1975) *Climatological Statistics for East Africa* (East African Meteorological Department, Nairobi, Kenya).

120. Altmann J, Alberts SC, Altmann SA, Roy SB (2002) Dramatic change in local climate patterns in the Amboseli basin, Kenya. *African Journal of Ecology* 40(3):248–251.

121. National Climatic Data Center (2014) National Climatic Data Center. Available at: http://www.ncdc.noaa.gov/cdo-web/datatools/findstation [Accessed June 7, 2014].

122. Yineger H, Kelbessa E, Bekele T, Lulekal E (2008) Floristic composition and structure of the dry Afromontane forest at Bale Mountains National Park, Ethiopia. *Ethiop J Sci* 31(2):103–120.

123. Ndey JA, Smith KH, Antoninova M (2014) Vegetation & Climate. *Garamba, Conservation in Peace and War*, eds Smith KH, Kalpers J, Arranz L, Ortega N, pp 3–18.

124. Makana J-R, Thomas SC (2005) Effects of Light Gaps and Litter Removal on the Seedling Performance of Six African Timber Species. *Biotropica* 37(2):227–237.

125. Makana J, Hart TB, Liengola I, Ewango C, Hart JA (2004) Ituri forest dynamics plots, Democratic Republic of Congo. *Flora of Tropical East Africa* (Balkema Publishers), pp 492–505.

126. Mugasha WA, et al. (2013) Allometric models for prediction of above- and belowground biomass of trees in the miombo woodlands of Tanzania. *Forest*

Ecology and Management 310(C):87–101.

127. Hartter J, Ryan SJ, Southworth J, Chapman CA (2011) Landscapes as continuous entities: forest disturbance and recovery in the Albertine Rift landscape. *Landscape Ecol* 26:877–890.

128. The Weather of East Africa. 1964-1971. East African Meterological Department. E. A. Community. Nairobi. *The Weather of East Africa. 1964-1971. East African Meterological Department. E. A. Community. Nairobi.*

129. Egeru A, et al. (2014) Assessing the spatio-temporal climate variability in semi-arid Karamoja subregion in north-eastern Uganda. *International Journal of Environmental Studies* 71:490–509.

130. Sinclair A, et al. (2008) Historical and future changes to the Serengeti ecosystem. *Serengeti III: Human Impacts on Ecosystem Dynamics*, eds Sinclair A, Packer C, Mduma SAR, Fryxell JM (University of Chicago Press, Chicago), pp 7–46.

131. Ngatia LW, et al. (2014) Seasonal patterns in decomposition and nutrient release from East African savanna grasses grown under contrasting nutrient conditions. *Agriculture, Ecosystems & Environment* 188:12–19.

132. Apio A, Muwanika V, Plath M (2009) Seasonal variation in reproductive behaviour of bushbuck (*Tragelaphus scriptus* Pallas, 1766) in an equatorial savannah ecosystem. *African Journal of Ecology* 47:592–597.

133. Averbeck C, Plath M, Wronski T, Apio A (2012) Effect of human nuisance on the social organisation of large mammals: group sizes and compositions of seven ungulate species in Lake Mburo National Park and the adjacent Ankole Ranching Scheme. *Wildlife Biology* 18(2):180–193.

134. Ogutu JO, Owen-Smith N, Piepho HP, Kuloba B (2012) Dynamics of ungulates in relation to climatic and land use changes in an insularized African savanna ecosystem. *Biodiversity and Conservation* 21:1033–1053.

135. Henschel P, Abernethy KA, White LJT (2005) Leopard food habits in the Lopé National Park, Gabon, Central Africa. *African Journal of Ecology* 43(1):21–28.

136. Demeke Y, Bekele A (2000) Population estimates and threats to elephants *Loxodonta africana* (Blumenbach 1797) in the Mago National Park, Ethiopia. *Tropical Zoology* 13:227–237.

137. Jacobs MJ, Schloeder CA (2002) Fire frequency and species associations in perennial grasslands of south-west Ethiopia. *African Journal of Ecology* 40(1):1–9.

138. Boutton TW, Tieszen LL, Imbamba SK (1988) Biomass dynamics of grassland vegetation in Kenya. *African Journal of Ecology* 26(2):89–101.

139. Ogutu JO, Piepho HP, Dublin HT (2012) Ostrich recruitment dynamics in relation to rainfall in the Mara–Serengeti ecosystem. *Ostrich* 83(3):119–136.

140. Rasmussen HB, Wittemyer G, Douglas-Hamilton I (2006) Predicting time-specific changes in demographic processes using remote-sensing data. *Journal of Applied Ecology* 43:366–376.

141. Thompson BW (1966) The mean annual rainfall of Mount Kenya. *Weather* 21:48–49.

142. Olupot W, Parry L, Gunness M, Plumptre AJ (2012) *Conservation Research in Uganda's Savannas* (Nova Science Publishers, New York).

143. Yusuf H, Treydte AC, Demissew S, Woldu Z (2011) Assessment of woody species encroachment in the grasslands of Nechisar National Park, Ethiopia. *African Journal of Ecology* 49(4):397–409.

144. Jaetzold R, Schmidt H, Hornetz B (1983) *Farm Management Handbook Of Kenya, Vol. II/C. East Kenya.* (Ministry of Agriculture, Kenya, in Cooperation with the German Agricultural Team (GAT) of the German Agency of Technical Cooperation (GTZ), Erhart GmbH, Trier).

145. Ejigu D, Bekele A (2014) Diurnal activity patterns and feeding ecology of the endemic geladas (Theropithecus gelada) in the Simien Mountains National Park, Ethiopia. *African Journal of Ecology* 53(2):231–237.

146. Walker A, Leakey RE, Harris JM, Brown FH (1986) 2.5-myr *Australopithecus boisei* from west of Lake Turkana, Kenya. *Nature* 322:517–522.

147. Roche H, et al. (2003) Les sites archéologiques plio-pléistocènes de la formation de Nachukui, Ouest-Turkana, Kenya: bilan synthétique 1997–2001. *Comptes Rendus Palevol* 2(8):663–673.

148. Brugal JP, Roche H, Kibunjia M (2003) Faunes et paléoenvironnements des principaux sites archéologiques plio-pléistocènes de la formation de Nachukui (Ouest-Turkana, Kenya). *Comptes Rendus Palevol* 2(8):675–684.

149. Prat S, Brugal JP, Roche H, Texier PJ (2003) Nouvelles découvertes de dents d'hominidés dans le membre Kaitio de la formation de Nachukui (1, 65–1, 9 Ma), Ouest du lac Turkana (Kenya). *Comptes Rendus Palevol* 2(8):685–693.

150. Leakey RE, Walker A (1988) New *Australopithecus boisei* specimens from east

and west Lake Turkana, Kenya. *American Journal of Physical Anthropology* 76(1):1–24.

151. McDougall I, Brown FH, Fleagle JG (2008) Sapropels and the age of hominins Omo I and II, Kibish, Ethiopia. *Journal of Human Evolution* 55(3):409–420.

Table S1: Location and climate of modern sites in eastern and central Africa.

Regions	Country	Lat	Long	Elevation	MAT (°C)	MAP (mm/y)	PET (mm/y)	WD (mm/y)	MW ($\delta^{18}O_{SMOW}$)	Climate Reference
Aberdares	Kenya	-0.43	36.70	2100-3000	11.6	1417	623	-794	-4.6	(119)
Amboseli	Kenya	-2.71	37.21	1140	24.0	346	1331	882	-5.2	(120)
Arabuko-Sokoke	Kenya	-3.23	39.88	60-135	26.1	850	1548	698	-2.3	(119)
Athi Plains	Kenya	-1.44	36.84	1640	19.4	741	865	124	-3.4	(121)
Awash NP	Ethiopia	9.09	40.03	1052	25.0	477	1361	884	-2.1	(121)
Bale Mtns	Ethiopia	6.75	39.75	3000-4000	9.0	1219	575	-644	-1.9	(122)
Garamba	DRC	4.00	29.50	800	24.4	1251	1276	25	-	(123)
Ituri Forest	DRC	1.38	28.58	770	22.4	1639	1063	-576	-2.3	(124, 125)
Kahuzi-Bega	DRC	-2.00	28.00	1800-2500	20.15	1607	905	-702	-	(121)
Katavi	Tanzania	-6.92	31.30	800-1100	18.0	950	1204	323	-3.8	(126)
Kibale	Uganda	0.60	30.40	900-1590	19.0	1662	845	-817	-1.7	(127, 128)
Kidepo	Uganda	3.74	33.72	1000-1300	24.5	427	1290	863	-	(129)
Kisumu	Kenya	-0.10	34.75	1157	23.2	1306	1139	-167	-3.3	(119)
Laetoli	Tanzania	-3.24	35.19	1500-2000	21.0	400	958	558	-3	(130)
Laikipia	Kenya	0.30	36.80	1700	21.8	640	1012	372	-3	(131)
Lake Edward	Uganda/ DRC	0.00	30.00	950	25.3	680	1406	726	-1.9	(132)
Lake Baringo	Kenya	0.57	36.00	1067	24.6	645	1303	658	-3.3	(119)
Lake Mburo	Uganda	-0.61	30.98	1210	21.3	887	975	88	-2.3	(133)
Lake Naivasha	Kenya	-0.71	36.36	1900	17.3	620	773	153	-2.4	(119)
Lake Nakuru	Kenya	-0.33	36.12	1870	17.7	869	787	-82	-3.3	(134)
Lake Turkana	Kenya	4.29	36.29	360-450	29.7	187	2572	2386	-1.5	(121)
Lopé	Gabon	-0.42	11.52	100-600	25.5	1492	1437	-55	-	(135)
Mago/Omo	Ethiopia	5.50	36.25	400	26.0	830	1522	692	-1.1	(136, 137)
Mara-Serengeti	Tanzania/ Kenya	-1.55	35.00	1500-2170	20.5	998	926	-72	-3.6	(138, 139)
Marsabit	Kenya	2.25	37.72	250-650	23.5	380	1169	789	-3.5	(119, 140)
Meru	Kenya	0.08	38.18	460	23.5	380	1169	789	-4.1	(119, 140)
Mount Kenya	Kenya	0.00	37.37	2500-3000	7.4	1250	552	-698	-3.8	(141)
Murchison Falls	Uganda	2.15	31.3	619-1291	25.5	1300	1437	137	-1.4	(142)
Narok	Kenya	-1.11	35.86	1890	16.5	736	746	10	-3.7	(119)
Nechisar	Ethiopia	5.95	37.67	1250-1360	23.9	1253	1216	-37	-2.0	(143)
Olorgesailie	Kenya	-1.58	36.44	619	29.0	417	2284	1867	-2.2	(119)
Samburu	Kenya	0.50	37.58	1100	23.5	380	1167	789	-2.9	(119, 140)
Shimba Hills	Kenya	-4.25	39.40	400	23.7	1150	1193	43	-2.3	(144)
Simien Mtns	Ethiopia	13.25	38.10	3100-3800	14.3	1054	682	-372	-1.9	(145)
Tana Delta	Kenya	-2.27	40.77	30	26.8	917	1689	772	-2.3	(119)
Tana River	Kenya	-0.47	39.63	138	28.8	363	2227	1864	-4.1	(121)
Tsavo	Kenya	-2.32	38.47	560	25.0	549	1348	799	-3.5	(119)

Table S2: Summary of fossil collections used in paleoaridity analysis.

Area	Locality	Formation/Bed	Age (Ma)	Key fossils or archaeology	Depositional context	Key References
Aramis (Middle Awash)	ARA-VP-1/6/17, KUS-VP-2, SAG-VP-7	Sagantole Fm., lower Aramis Mb.	4.419-4.416	*Ardipithecus ramidus*	Alluvial floodplain	(92, 93)
Kanapoi		Kanapoi Fm.	4.20-4.11	*Australopithecus anamensis*	Fluviolacustrine	(75, 77)
Allia Bay	261-1	Koobi Fora Fm., Upper Lonyumun Mb.	4.02-3.97	*Australopithecus anamensis*	Fluvial	(75)
Lomekwi (West Turkana)	LO4/5	Nachukui Fm., lower Lomekwi Mb.	3.41-3.36	*Kenyanthropus platyops*	Fluvial	(66, 79)
Kangatu-kuseo	KU2/3	Nachukui Fm., upper Lomekwi Mb.	2.53	*Paranthropus aethiopicus*	Fluvial	(66, 146)
Kangatu-kuseo	KU1	Nachukui Fm., upper Lomekwi/ Lokalalei Mb.	3.07-2.53		Fluvial	(66)
Kokiselei (West Turkana)	KS2	Nachukui Fm., Kalochoro Mb.	2.33-1.87	Oldowan lithics	Fluvial/Marginal lacustrine	(147, 148)
Kanjera South (Homa Peninsula)	KS-2	Kanjera Fm., Southern Mb., Bed 2	2.0	Oldowan lithics, hominin omnivory (prey bone modification and lithic use-wear studies)	Fluvial/Aeolian	(70, 97, 98, 104)
Koobi Fora (East Turkana)	FwJj20	Koobi Fora Fm., upper Burgi Mb.	1.95	Oldowan lithics, hominin omnivory (prey bone modification)	Fluvial-deltaic	(80)
Kokiselei (West Turkana)	KS1	Nachukui Fm., Kaitio Mb.	1.87-1.76	*Paranthropus boisei,* Oldowan lithics	Fluvial/Marginal lacustrine	(147-149)
Kalochoro, Loruth Kaado, Naiyena Engol (West Turkana)	KL3/6, NY2/3	Nachukui Fm., Kaitio Mb.	1.87-1.30	*Paranthropus boisei, Homo* sp., Oldowan lithics	Fluvial	(66, 73, 147-150)
Kibish	006, 052, 061, 069, 073, 082, 086, 103, 106, 171	Kibish Fm., Mb. 1	0.196	*Homo sapiens*, Middle Stone Age lithics	Deltaic	(84-86, 108, 151)
Kibish	126, 185	Kibish Fm., Mb. 4	0.013-0.004	Bone artifacts and possibly human fossils	Deltaic	(84, 111)

Table S3: Oxygen isotopic enrichment between ES and EI taxa (ε_{ES-EI}) and water deficit (WD) calculations for fossil collections.

Locality	$\varepsilon_{Giraffe-Hippo}$	$WD_{Gir-Hippo}$	$\varepsilon_{Tragelaphini-Hippo}$	$WD_{Trag-Hippo}$	$\varepsilon_{Hippotragini-Hippo}$	$WD_{Hipp-Hippo}$	$\varepsilon_{Tragelaphini-Eleph}$	$WD_{Trag-Eleph}$	$\varepsilon_{Tragelaphini-Rhino}$	$WD_{Trag-Rhino}$	mean WD_{ES-EI}
Aramis (ARA-VP-1/6/17, KUS-VP-2, SAG-VP-7)	9.3 ± 3.0	1483 ± 1097	4.7 ± 4.1	194 ± 902	7.2 ± 3.1	1733 ± 1039	1.4 ± 3.1	157 ± 803	0.3 ± 4.2	-55 ± 1083	702 ± 2217
Kanapoi	8.8 ± 2.6	1315 ± 994	-	-	-	-	-	-	-	-	1315 ± 994
Allia Bay (261-1)	6.4 ± 3.7	500 ± 1315	2.0 ± 4.0	-365 ± 889	-	-	-0.2 ± 4.3	-237 ± 1058	-3.2 ± 3.8	-917 ± 994	-255 ± 2151
Lomekwi (LO4/5)	5.0 ± 2.3	1 ± 892	-	-	1.9 ± 1.1	54 ± 490	-	-	-	-	28 ± 1018
Kangatukuseo (KU2/3)	-	-	-	-	-	-	0.4 ± 0.9	-99 ± 388	-	-	-99 ± 388
Kangatukuseo (KU1)	9.9 ± 0.0	1693 ± 423	-	-	-	-	-	-	-	-	1693 ± 423
Kanjera South (KS-2)	-	-	1.1 ± 1.1	-534 ± 395	-	-	-	-	-	-	-534 ± 395
Il Dura (FwJj20)	-	-	-	-	5.9 ± 0.6	1311 ± 393	-	-	-	-	1311 ± 393
Kokiselei (KS1)	-	-	1.1 ± 2.0	-547 ± 519	-	-	-	-	0.3 ± 1.4	-66 ± 466	-307 ± 698
Kokiselei (KS2)	-	-	-	-	-	-	-	-	0.3 ± 0.8	-54 ± 360	-54 ± 360
Kalochoro KL3/6, Naiyena Engol NY2/3	-	-			5.3 ± 1.4	1123 ± 575					1123 ± 575
Kibish Fm. Mb. 4 (126, 185)	-	-	-	-	4.5 ± 0	876 ± 346	-	-	-	-	876 ± 346
Kibish Fm. Mb. 1 (006, 052, 061, 069, 073, 082, 086, 103, 106, 106, 171)	5.6 ± 2.6	216 ± 981	5.1 ± 2.6	272 ± 627	3.3 ± 2.2	496 ± 785	-	-	-	-	328 ± 1404

Table S4. Aridity index equations (WD-$\varepsilon_{ES\text{-}EI}$ regressions) describing statistically significant ($p < 0.05$) relationships between water deficit (WD) and the oxygen isotopic enrichment (ε) between evaporation sensitive and evaporation insensitive taxa (Figure 3).

Linear model	Residual standard error of the regression	Standard error of the regression coefficient
$WD = \varepsilon_{Giraffidae-Hippopotamidae} * 340.9 - 1686.5$	478.1	63.42
$WD = \varepsilon_{Tragelaphini-Hippopotamidae} * 204.3 - 766.0$	344.4	29.69
$WD = \varepsilon_{Hippotragini-Hippopotamidae} * 316.9 - 561.4$	340.4	62.48
$WD = \varepsilon_{Tragelaphini-Elephantidae} * 237.2 - 184.8$	333.3	31.52
$WD = \varepsilon_{Tragelaphini-Rhinocerotidae} * 246.6 - 134.3$	193.1	21.47

Table S5. Average $\delta^{13}C_{enamel}$ values for fossil Artiodatyla, Perissodactyla, and Proboscidea in eastern African paleoaridity fossil collections, calculated following (56). Compilation of $\delta^{13}C_{enamel}$ values used here is presented in Dataset S4. Percent G, M, and B calculations exclude gen. sp. indet in families with identified tribes or genera.

		Aramis	Kanapoi	Allia Bay	Lomekwi	Kangatukuseo	Kangatu-kuseo	Kokiselei	Koobi Fora	Kokiselei	Kalochoro/ Naiyena Engol	Kanjera S.	Kibish	Kibish
				261-1	LO4/5	KU1	KU2/3	KS2	FwJj20	KS1	KL3/6, NY 2/3	KS-2	Mb1	Mb4
Artiodactyla	n													
Bovidae														
Aepycerotini	41	-2.4	-1.9	-5.8	-1.2				1.0	-1.7	-0.6			
Alcelaphini	75	-0.5	1.5	-0.3	0.8	1.0	0.9	2.6	2.2	1.2	1.8	2.6	0.4	
Antilopini	28			-7.6	-3.2							1.3	-8.9	
Bovini	24	-0.5						2.4		0.0		1.8	0.0	-0.2
Hippotragini	14	0.2			-3.6		0.0		2.5	2.7	1.1		0.6	-2.4
Neotragini	5	-9.6	-11.6											
Reduncini	31						0.0	3.0	1.7	1.1		1.3	-0.2	1.3
Tragelaphini	50	-9.8	-8.1	-7.7	-5.9		-8.3			-4.8	-3.3	-2.1	-9.9	
indet	8													
Giraffidae														
Giraffa	19	-12.1	-11.5	-11.3	-11.2	-11.5							-4.4	
Sivatherium	12	-11.9	-8.9	-12.2	-11.3		-9.8							
indet	7							0.1	-12.2					
Hippopotamidae	99	-2.5	-2.0	-3.4	-3.9	-2.2	-3.2		0.0	-1.6	2.4	1.3	-2.8	-4.3
Suidae														
Notochoerus	8		-3.9						-0.4					
Nyanzachoerus	19	-1.2	-1.6	-4.4										
Potamochoerus/ Kolpochoerus/ Hylochoerus	16	-6.4							0.3	-4.0			-0.9	
Metridiochoerus/ Phacochoerus	33							-0.2	-0.4	-0.5		0.3	0.3	-1.0
indet	2													
Perissodactyla														
Equidae														
Equus	18							0.6	0.0	-1.9		1.5	0.9	
Hipparion/ Eurygnathohippus	20	0.6	1.2						1.0	0.2		1.5		
Rhinocerotidae														
Ceratotherium/ Rhino G	21	1.0						1.6		0.2				
Diceros/Rhino MB	24	-4.7	-9.0	-10.0	-5.7									
indet									1.5					
Proboscidea														
Deinotheriidae														
Deinotherium	22	-12.5	-12.4	-12.7	-11.1	-13.4				-7.5				
Gomphotheriidae														
Anancus	6	-0.4	-0.1											
Elephantidae														
Elephas	18		-2.7		-0.6		0.5				0.0			
Loxodonta	10		-2.4	-1.8	-1.7		0.4				0.3			
indet	21	-1.7							0.0					
	n (taxa)	17	15	11	12	4	8	7	13	13	7	9	11	5
	G (%)	35	20	9	17	25	63	100	92	54	86	89	64	60
	M (%)	35	40	55	58	25	13	0	0	46	14	11	18	40
	B (%)	29	40	36	25	50	25	0	8	0	0	0	18	0

Figure S1: Modern climate data. Revised potential evapotranspiration (PET) and water deficit (WD) calculations used in this study (black circles) compared to previous (8) calculations (gray circles), plotted with measured mean annual precipitation (MAP) (left column) and mean annual temperature (MAT) (right column).

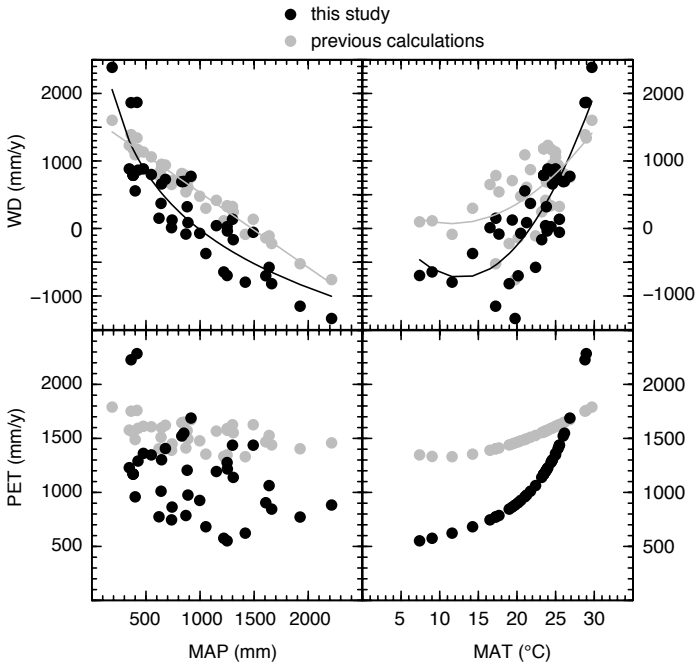

Figure S2: Oxygen isotopic composition of oxygen sources and modern EI and ES taxa. (A) $\delta^{18}O$ values of atmospheric oxygen and meteoric water. (B) $\varepsilon_{leaf\text{-}mw}$ values for leaf water and leaf cellulose. (C) $\varepsilon_{enamel\text{-}mw}$ of EI taxa. (D) $\varepsilon_{enamel\text{-}mw}$ of ES taxa. Arrows below the x-axis in (C) and (D) depict the direction of change for major oxygen influxes (drinking water, leaf water) in body water model predictions depicted by lines in (C) and (D). Error in (C) and (D) represents propagated error of measured $\delta^{18}O_{enamel}$ and $\delta^{18}O_{mw}$ values.

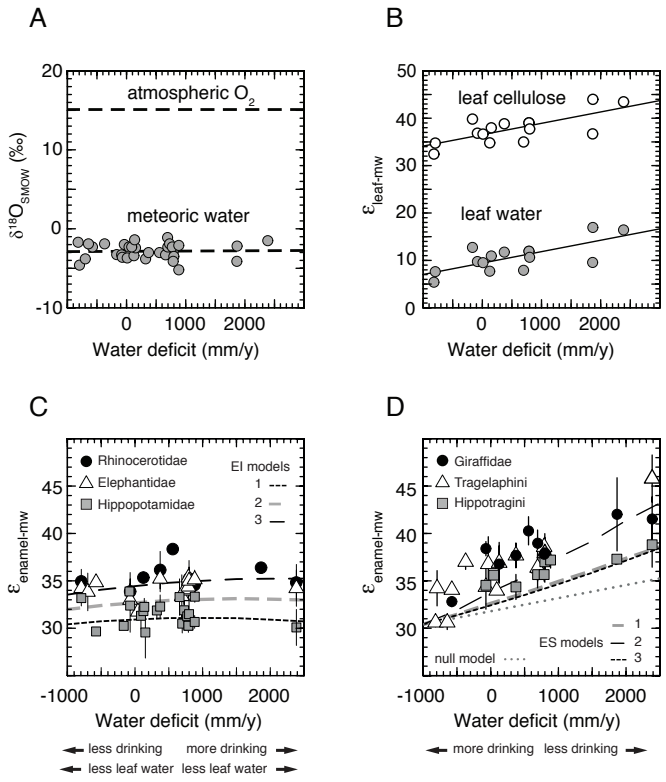

Figure S3: Formations and major tuffs from the Kanapoi Formation, Koobi Fora Formation, Nachukui Formation, and Kibish Formation. Chronology and tephra correlations (marked as thin lines between tuffs) based on (64). The geomagnetic scale (113) is included on the time scale for reference. Gray bars represent members of each formation (73). Fossil collections, labeled in italics, are placed in approximate stratigraphic position.

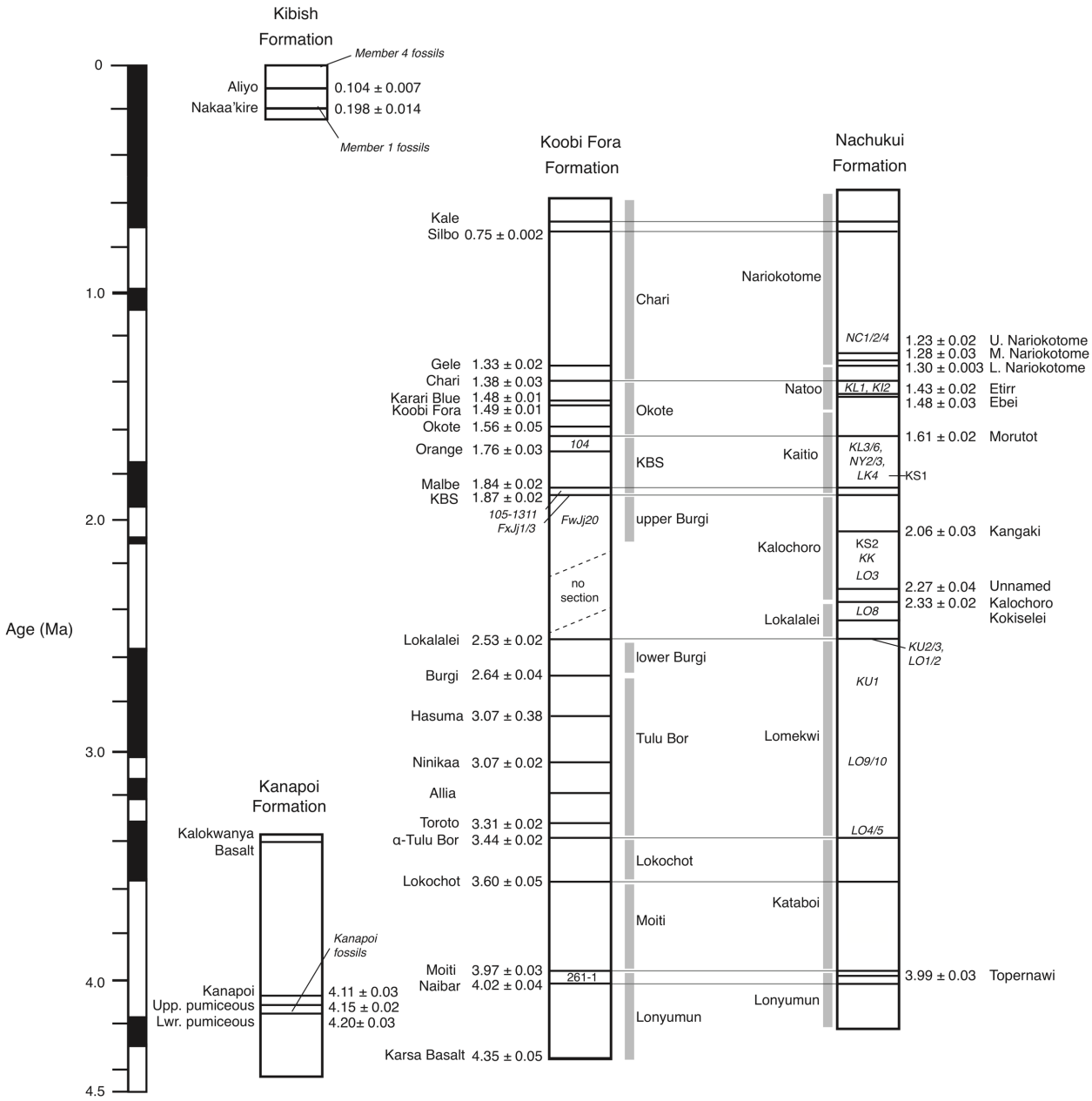

Figure S4. Paleoaridity from eastern African fossil collections, expressed as water deficit (mm/y) calculated using $\varepsilon_{ES\text{-}EI}$ regressions (Fig. 3 and Table S4) using (A) all available pairs of evaporation sensitive (ES) and evaporation insensitive (EI) taxa, (B) Hippopotamidae as the EI taxon, and (C) Elephantidea and Rhinocerotidae as EI taxa. Error bars indicate uncertainty in age and propagated error in water deficit estimates (see SI discussion). Shapes indicate geographic region and colors indicate pairs of ES and EI taxa. Gray open shapes indicate the mean water deficit calculated from multiple $\varepsilon_{ES\text{-}EI}$ values, and gray error bars indicate total propagated error of the mean WD values. Water deficit values without an open gray shape represent a single $\varepsilon_{ES\text{-}EI}$ value.

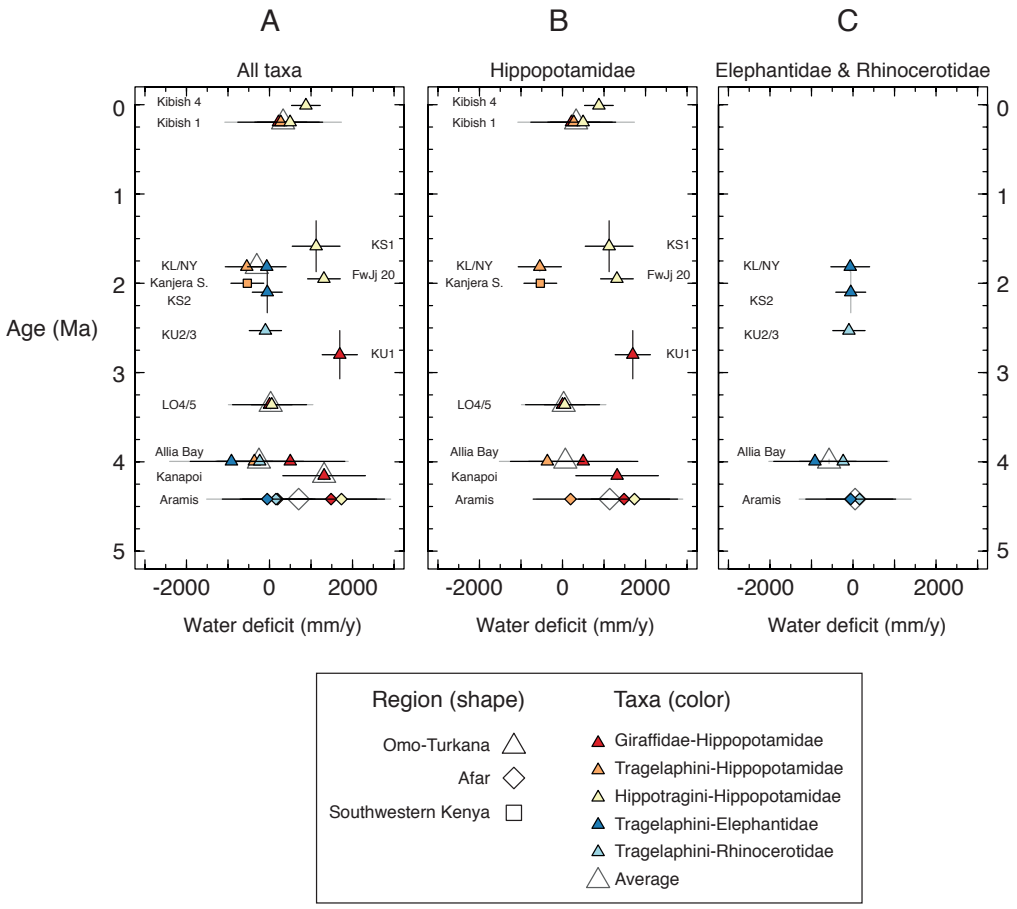

Figure S5. Percent C_4 grazers among large mammalian herbivores in the Omo-Turkana Basin calculated using $\delta^{13}C_{enamel}$ values from paleoaridity "snapshot" fossil collections compared to calculations using $\delta^{13}C_{enamel}$ values from a larger compilation of fossils from Turkana binned into large time intervals (>100 kyr). $\delta^{13}C_{enamel}$ values and $\%C_4$ grazer calcuations from paleoaridity fossil collections are available in Table S5 and Dataset S4, and $\%C_4$ grazers in time bins are taken from (56), with the addition of data from the Omo Mursi Formation (88) and Shungura Formation (83).

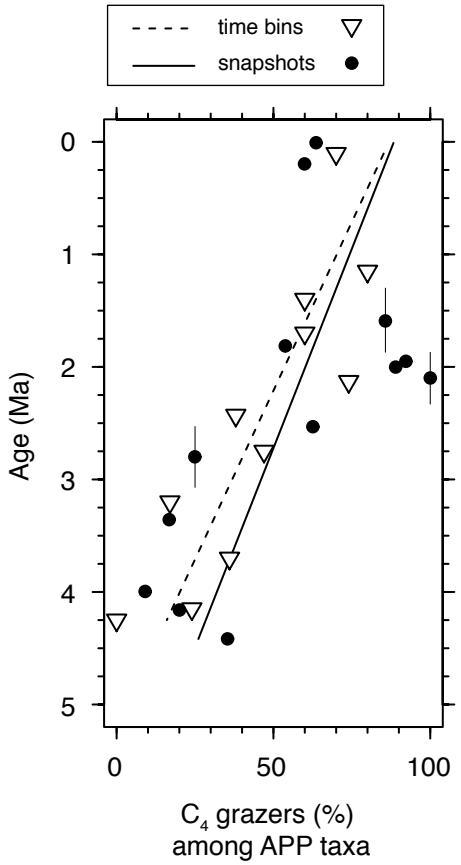

Figure S6. Compilation of paleoclimate indicators from the Omo-Turkana Basin, Kenya. (A) Water deficit (mm/y) calculated using fossil tooth enamel $\delta^{18}O$ values and $\varepsilon_{ES\text{-}EI}$ regressions for all available pairs of evaporation sensitive and evaporation insensitive taxa. (B) Precipitation (mm/y) calculated from paleosol depth to calcic horizon (114). (C) Precipitation (mm/y) calculated from mammal taxonomic community structure (115). (D) Percent Alcelaphini and Antilopini (AA) among bovid tribes (116). (E) Precipitation (mm/y) calculated from mammal dental morphology (hypsodonty and lophedness) using a linear regression model (117). (F) Precipitation (mm/y) calculated from mammal dental morphology (hypsodonty and lophedness) using a k-nearest neighbor model (117).

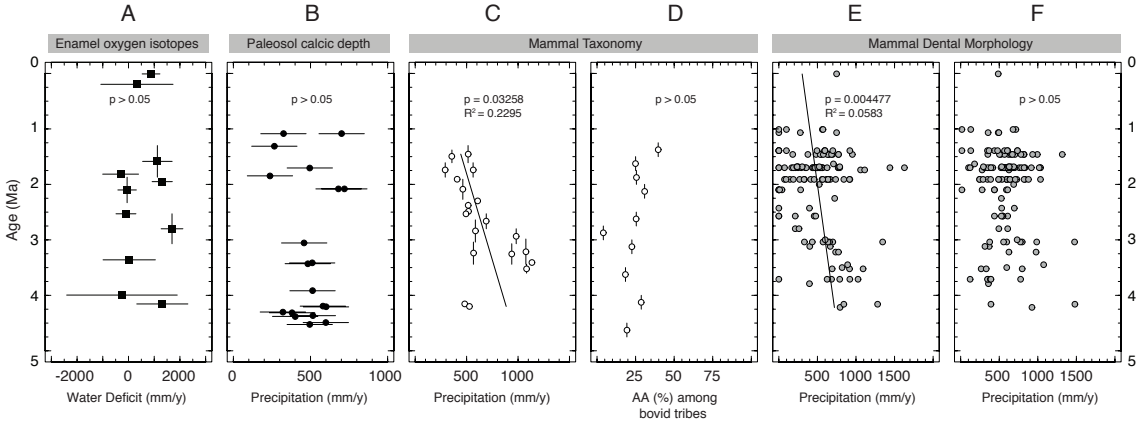

Figure S7: $\delta^{18}O$ values in fossil evaporation insensitive (EI) taxa and paleosol carbonates from the Omo-Turkana Basin, Kenya. (A) Individual $\delta^{18}O$ values (see Dataset S3) in fossil EI taxa from the Omo-Turkana Basin. (B) $\delta^{18}O$ values in fossil EI taxa from paleoaridity fossil collections. Error bars represent the standard error of mean $\delta^{18}O$ values and age uncertainty. (C) Left, paleosol carbonate $\delta^{18}O$ values (open circles) (118) and binned by 50 kyr time intervals (gray circles); Right, estimated paleo-soil water $\delta^{18}O$ values (12).

A. Omo-Turkana Basin fossils

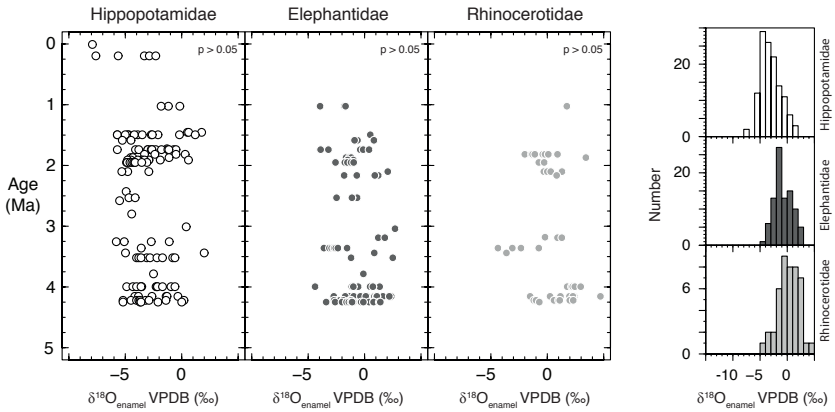

B. Omo-Turkana Basin paleoaridity fossil collections

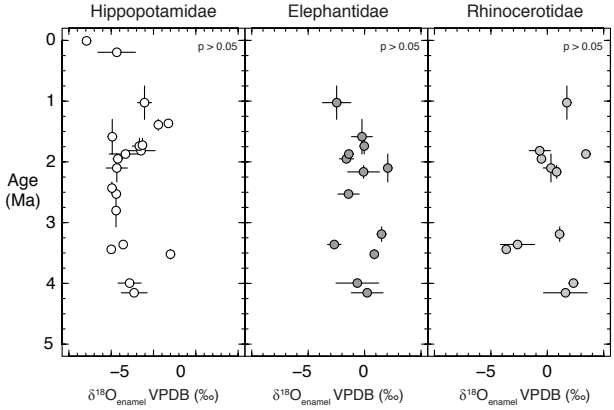

C. Omo-Turkana Basin paleosol carbonates

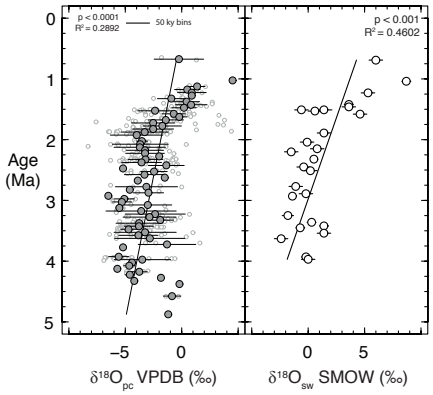

Figure S8: $\delta^{18}O$ values in fossil (A) evaporation insensitive taxa and (B) evaporation sensitive taxa from paleoaridity fossil collections in eastern Africa. Error bars represent the standard error of mean $\delta^{18}O$ values and age uncertainty. (C) $\varepsilon_{ES\text{-}EI}$ values in paleoaridity fossil collections. Error bars represent propagated uncertainty of $\varepsilon_{ES\text{-}EI}$ values and age uncertainty. Shapes represent geographic region. Omo-Turkana sites are the open triangles, Afar site is the closed diamond, and southwestern Kenya site is the grey square (see legend).